Check for updates

Received: 2 January 2022 | Revised: 24 February 2022 | Accepted: 25 February 2022

DOI: 10.1002/cey2.200

REVIEW

CARBON ENERGY WILEY

Flexible MXene films for batteries and beyond

Yang Huang[1] | Qiongqiong Lu[2] | Dianlun Wu[1] | Yue Jiang[1] | Zhenjie Liu[1] | Bin Chen[1] | Minshen Zhu[3] | Oliver G. Schmidt[3,4,5]

[1]Shenzhen Key Laboratory of Polymer Science and Technology, College of Materials Science and Engineering, Shenzhen University, Shenzhen, China

[2]Institute for Complex Materials, Leibniz IFW Dresden, Dresden, Germany

[3]Center for Materials, Architectures, and Integration of Nanomembranes (MAIN), Chemnitz University of Technology, Chemnitz, Germany

[4]Material Systems for Nanoelectronics, Chemnitz University of Technology, Chemnitz, Germany

[5]School of Science, Dresden University of Technology, Dresden, Germany

Correspondence
Yang Huang, Shenzhen Key Laboratory of Polymer Science and Technology, College of Materials Science and Engineering, Shenzhen University, 518055 Shenzhen, China.
Email: y.huang@outlook.com

Minshen Zhu, Center for Materials, Architectures, and Integration of Nanomembranes (MAIN), Chemnitz University of Technology, 09126 Chemnitz, Germany.
Email: minshen.zhu@main.tu-chemnitz.de

Funding information
National Natural Science Foundation of China, Grant/Award Number: 52002247; Deutsche Forschungsgemeinschaft, Grant/Award Number: ZH 989/2-1; Natural Science Foundation of Guangdong Province, Grant/Award Number: 2019A1515011344

Abstract

MXenes add dozens of metallic conductors to the family of two-dimensional (2D) materials. A top-down synthesis approach removing A-layer atoms (e.g., Al, Si, and Ga) in MAX phases to produce 2D flakes attaches various surface terminations to MXenes. With these terminations, MXenes show tunable properties, promising a range of applications from energy storage devices to electronics, including sensors, transistors, and antennas. MXenes are also excellent building blocks to create flexible films used for flexible and wearable devices. This article summarizes the synthesis of MXene flakes and highlights aspects that need attention for flexible devices. Rather than listing the development of energy storage devices in detail, we focus on the main challenges of and solutions for constructing high-performance devices. Moreover, we show the applications of MXene films in electronics to call on designs to construct a complete system based on MXene with good flexibility, which consists of a power source, sensors, transistors, and wireless communications.

KEYWORDS
2D materials, flexible batteries, flexible electronics, intelligent system, MXene

1 | INTRODUCTION

Two-dimensional (2D) materials have attracted considerable attention because of their unique mechanical, optical, thermal, magnetic, and electronic properties compared to their bulky and multilayered counterparts.[1–3] As the pioneer of 2D materials, graphene has shown broad application potential in the fields of sensors, catalysts, energy storage, and electronic devices.[1,2,4,5] In addition to graphene, dozens of other 2D materials are synthesized

Yang Huang, Qiongqiong Lu, and Dianlun Wu contributed equally to this study.

This is an open access article under the terms of the Creative Commons Attribution License, which permits use, distribution and reproduction in any medium, provided the original work is properly cited.
© 2022 The Authors. *Carbon Energy* published by Wenzhou University and John Wiley & Sons Australia, Ltd.

via top-down or bottom-up approaches,[6] including boron nitride,[7] metal chalcogenides,[8] phosphorene,[9,10] and 2D polymers.[11,12] To date, the family of 2D materials already consists of over 150 members while hundreds of companions by changing transition metal components are predicted to join, which ranges from metals, semimetals, semiconductors to insulators.[13] Apparently, 2D materials are one of the most challenging and exciting research fields in the 21st century. In 2011, titanium carbide (Ti_3C_2) was obtained by selectively etching the aluminum layer of titanium aluminum carbide (Ti_3AlC_2) in hydrofluoric acid (HF) for the first time.[14] Afterwards, more than 30 similar 2D transition metal carbides, nitrides, and carbonitrides were discovered,[15–17] yielding a large family of 2D materials, known as MXenes. The general formula of MXenes is $M_{n+1}X_nT_x$ ($n = 1–4$), where M and X represent early transition metals and carbon or nitrogen, respectively. T_x (x is variable) suggests termination groups on the outer surface of transition metals (Figure 1).[16,18,19] The M atoms of MXene crystals are close-packed, while the X atoms occupy the octahedral interstitial sites, forming a hexagonal close-packed structure with a $P6_3/mmc$ space group symmetry.[18]

Because free electrons can be provided by transition metals and act as carriers,[20,21] MXenes are more conductive than many other 2D materials (e.g., phosphorene and molybdenum disulfide). For example, some $Ti_3C_2T_x$ nanosheets with fewer defects can reach a high conductivity of 20,000 S cm^{-1}.[22] Moreover, the abundant surface termination groups of MXenes allow them to be highly hydrophilic, which is in sharp contrast to many hydrophobic 2D materials (e.g., graphene).[23,24] With the assistance of this hydrophilicity, combinations between MXenes and other materials can be easily achieved using diverse methods,[25,26] which provides many possibilities of research for various research communities, ranging from materials scientists to physicists. Based on their high conductivity, synthetic versatility, and expected advantages of 2D materials (e.g., flexibility and large surface area), MXenes have shown promising application potential in many fields, such as energy storage,[27–29] catalysis,[30] electromagnetic interface shielding,[31] and medicine.[32]

Using MXenes as the electrode material in electrochemical energy storage, batteries and supercapacitors have become a primary area of research over their

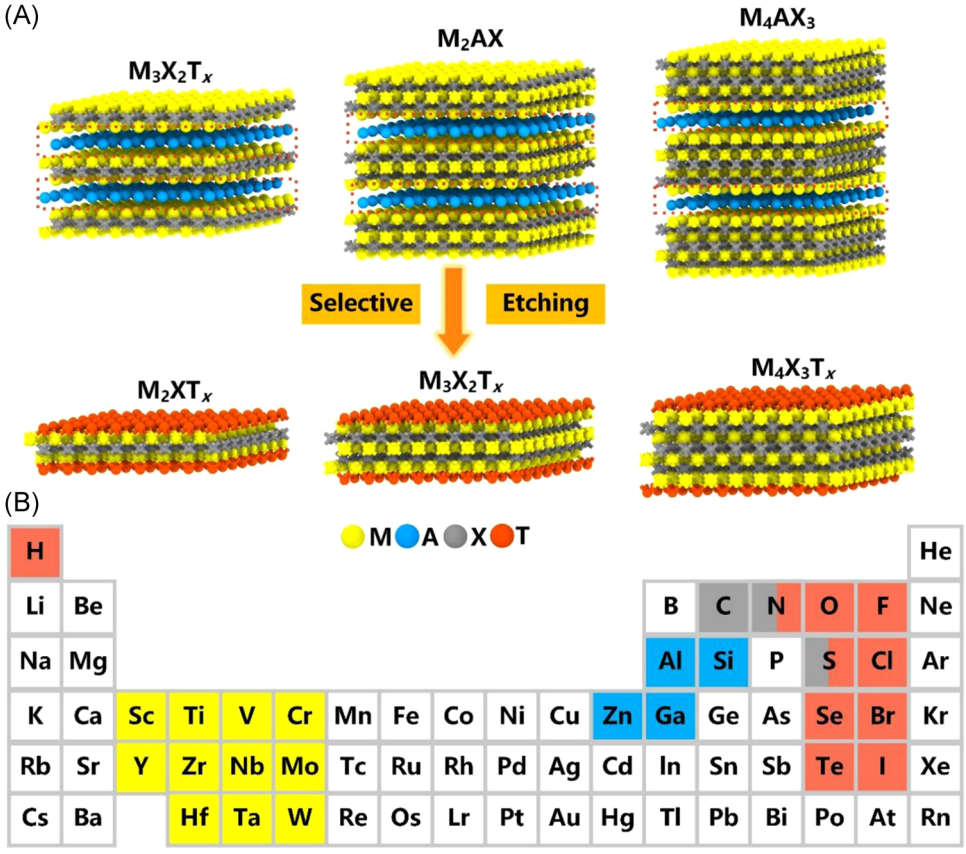

FIGURE 1 (A) Structural diagrams of MAX phases and corresponding MXenes after selective etching. (B) Periodic table of elements that have experimentally existed in MAX phases and MXenes. The elements of M, A, X, and T are colored according to the structural diagrams of (A)

10 years' development (from 2011 to 2022).[16,28] The metal transition core layer and the transition metal oxide-like outer surface of MXenes provide highways for electron transport and massive distributions of redox-active sites. The synergistic effects of these two inherent advantages allow MXenes to realize ultrafast charge storage that is good for high-rate applications.[19,28,33–35] Furthermore, MXenes are available for diverse redox chemistries by modifying their surface terminations, which produces high capacity and additional functionality.[20,29] Such extensibility of MXenes is rarely seen in most 2D materials and therefore provides solutions for developing batteries involving complex electrochemistry.[29] Therefore, MXenes have been widely used in different battery systems such as metal–ion, metal–sulfur, and metal–oxygen batteries. They can also offer more functions, such as inhibiting dendrite growth.[23,36,37]

In addition to the performance improvements (e.g., high capacity and rate capability), the application of MXenes promises outstanding flexibility. In contrast to a traditional battery with rigid packaging, a flexible battery can fulfill the requirements of portable or wearable electronics, which are becoming increasingly popular and expected to be bendable, foldable, twistable, and stretchable for everyday use. Flexible electrodes are one of the key components in flexible batteries that largely determine electromechanical performance. Taking advantage of high conductivity, flexibility, and mechanical stability, MXenes have been fabricated into flexible electrodes with different shapes, such as fibers, films/papers, and sponges, which can be readily used for flexible batteries.[27,38–40] The electromechanical performance of flexible batteries will be significantly enhanced by skillfully using MXenes.[29,41,42] Moreover, additional functions can be incorporated into the flexible batteries by tailoring the properties of MXene-based electrodes (e.g., self-healing and self-charging capabilities),[43–45] which can improve the practicality of batteries to a large degree.

Besides electrochemical properties for energy storage, MXenes have extensive possibilities for use in electronics. Basically, MXenes without surface terminations are highly conductive, which is enabled by free electrons of transition metals. As such, MXenes can be used as current collectors and interconnects. Abundant surface termination groups allow for the tunability of electronic properties: −OH decreases the work function, −O increases it, and −F affects it depending on the transition metals. Schottky-barrier-free hole or electron injection into semiconductors connected to MXenes is predicted, offering a new solution for improving electronics.[46] Various transition metals in MXenes offer additional possibilities. Mo-, Nb-, and V-based MXenes show semiconductor-like behavior.[47,48] In addition, substitution of outer Ti layers of $Ti_3C_2T_x$ by Mo also leads to semiconductor-like behavior.[49] From the engineering aspects, MXene flakes have been fabricated into suitable inks for printing, a commercially manufacturable way to develop flexible electronics. Therefore, MXenes show potential applications beyond energy storage devices.

This review focuses on the challenges of using MXenes in flexible batteries and their potential for integration into flexible electronics. Starting with an overview of the synthesis and processing of MXenes, we discuss the characteristics of different methods and corresponding effects on the structure and surface chemistry of MXenes. Then, the challenges in improving flexible battery performance are summarized and potential solutions are explored. Afterward, we review MXene films used for flexible electronics and show the possibility for integration. Finally, a description of the current challenges and future outlooks in relation to MXene-based flexible batteries is presented. We hope that this review will promote fast development of MXenes in designing high-performance batteries and further integration into flexible electronics.

2 | SYNTHESIS AND PROCESSING OF MXENES

Synthesis and processing of MXenes represent the first step in the fabrication of flexible batteries. In sharp contrast to other 2D materials, MXenes are not held together by van der Waals bonds in their parent MAX phases (Figure 1). In fact, the monoatomic A-layer atoms of MAX, mostly group 13 and 14 elements (e.g., Al, Si, and Ga), are the bridge between MXene monolayers. MXenes can be obtained by extracting A elements from MAX phases. This process is theoretically possible, considering the different chemical reactivities between metallic M–A bonds and mixed metallic/ionic/covalent M–X bonds in MAX ceramics.[19,50] In 2011, $Ti_3C_2T_x$, the first reported MXene, was experimentally achieved by etching the Al atomic layers of Ti_3AlC_2 in HF.[14] The resultant $Ti_3C_2T_x$ showed an accordion-like structure with multiple layers held by van der Waals and hydrogen bonds, as shown in Figure 2A–C.[51] Despite its different morphology, this $Ti_3C_2T_x$ retains the stoichiometry of Ti and C as the Ti_3AlC_2 precursor. Functional groups of –F, –OH, and –O are linked to the surface (Figure 2D).

Note that the etching process of $Ti_3C_2T_x$ is not a general approach for other MXenes because the reactivity of each MAX phase varies in terms of their variable bonding strengths between M–A and M–X.

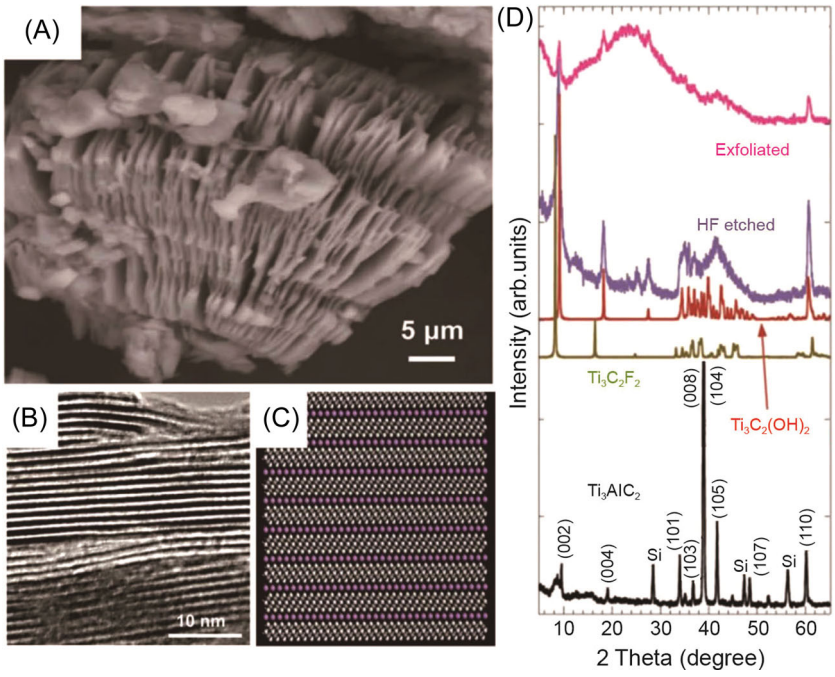

FIGURE 2 (A) Scanning electron microscopy (SEM) image of multilayer $Ti_3C_2T_x$ with an accordion-like morphology obtained by hydrofluoric acid (HF) etching. (B) Transmission electron microscopy image of multilayer $Ti_3C_2T_x$. (C) Atomic model of $Ti_3C_2T_x$ after Li insertion ($Ti_3C_2Li_2$). (D) Measured X-ray diffraction (XRD) patterns of Ti_3AlC_2, simulated XRD patterns of $Ti_3C_2F_2$ and $Ti_3C_2(OH)_2$, and measured XRD patterns of $Ti_3C_2T_x$ obtained by etching and exfoliation. Reproduced with permission: Copyright 2011, Wiley-VCH[14]

Thus, high-quality etching methods are still a research hotspot for the MXene family, which is the cornerstone for MXene-based flexible batteries.

The application of multilayer MXenes in some areas, for example, medicine and nanoelectronics,[32,52] can be severely limited due to their bulky size. Thus, intercalation and subsequent delamination are needed to obtain single- or few-layer nanosheets. These MXene flakes can be easily assembled into freestanding electrodes, which is favorable for flexible batteries. However, due to the strong interaction between MXene layers, the yield of MXene nanosheets can be low sometimes. As a result, various optimized strategies have been introduced to achieve a high yield of MXene nanosheets,[53,54] which could even support large-scale production.[55] In this subsection, the synthesis and processing of MXenes are reviewed by dividing them into two parts, namely, etching strategies and intercalation and delamination strategies. Their potential roles in the application of MXenes in flexible batteries are also discussed.

2.1 | Etching strategies of MXenes

The successful etching of $Ti_3C_2T_x$ was first achieved using HF at room temperature.[14] Then, a number of MXenes were obtained using this HF etching method, but with different HF concentrations, etching times, and etching temperatures. Some experimental results suggest that higher HF concentrations could shorten the etching time and improve the etching efficiency (Figure 3A,B).[58] Meanwhile, the etching temperature and time could play essential roles in obtaining multilayer MXenes (Figure 3C,D).[56] However, increasing the etchant concentration, etching temperature, and time blindly will lead to rapid development of defects and significantly reduced lateral sizes of MXenes, because HF is highly corrosive (Figure 3E–H).[57] Therefore, etching conditions for MXenes should be adjusted according to their desired properties and applications. As for flexible batteries, it is optimal for MXenes to have large lateral sizes and few defects, ensuring high conductivity and good structural stability, which determine the rate capability and cyclability to a large degree. Thus, to design a high-performance MXene-based flexible battery, mild conditions of the HF etching method, such as low HF concentrations, short etching time, and low etching temperatures, should be chosen to synthesize MXenes. The appearance of an accordion-like morphology is frequently mistaken for a sign of successful etching of MXenes, rather than the changes of the XRD pattern. In fact, this accordion-like structure is mainly attributed to the release of hydrogen gas during the etching process,[19,50,59] which cannot directly indicate the degree of etching of MXenes. Thus, making good use of XRD, where the diffraction peak of (*00l*) planes would broaden and downshift to a lower angle due to an increased interlayer spacing, is beneficial for the synthesis of MXenes with suitable properties for high-performance flexible batteries.

Abundant –F groups are terminated on the outer surface of MXenes after etching, which impairs conductivity.[16,60]

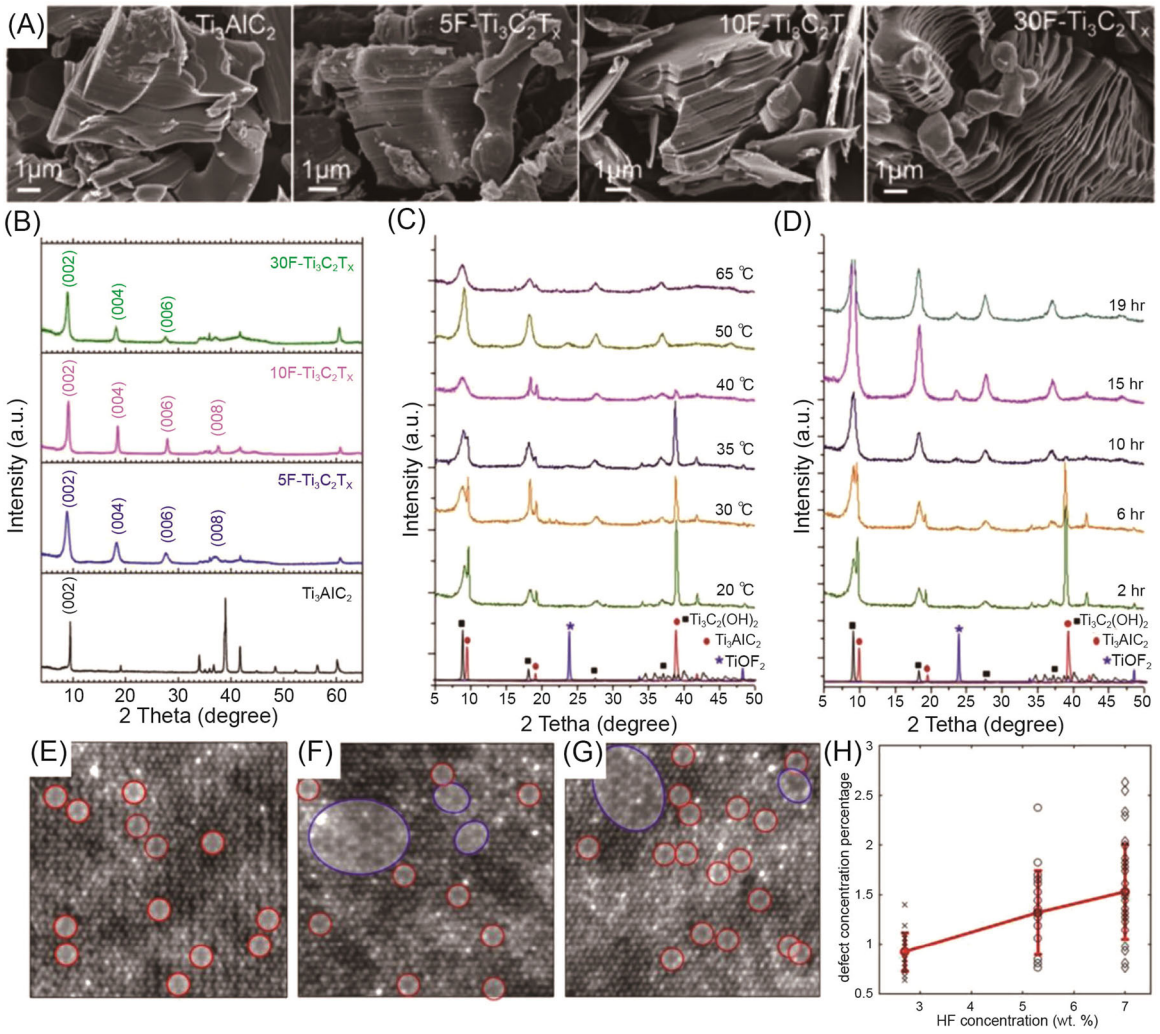

FIGURE 3 (A) Scanning electron microscopy images of Ti_3AlC_2 after etching with 5, 10, and 30 wt% hydrofluoric acid (HF). The accordion-like morphology could only be observed for the 30 wt% HF etched sample. (B) X-ray diffraction (XRD) patterns of Ti_3AlC_2 and resulting $Ti_3C_2T_x$ obtained after etching with 5, 10, and 30 wt% HF. Reproduced with permission: Copyright 2017, American Chemical Society.[56] XRD patterns of Ti_3AlC_2 after etching with a 50% HF solution as a function of (C) temperature after 2 h and (D) time at room temperature. Reproduced with permission: Copyright 2013, Elsevier.[56] High-angle annular dark-field scanning transmission electron microscopy images from single-layer $Ti_3C_2T_x$ obtained using etchants with different HF concentrations: (E) 2.7 wt% HF, (F) 5.3 wt% HF, and (G) 7 wt% HF. Single Ti vacancies and Ti vacancy clusters are indicated as red and blue circles, respectively. (H) Scatter plot of defect concentration from images acquired from $Ti_3C_2T_x$ obtained by different HF concentrations. Reproduced with permission: Copyright 2016, American Chemical Society[57]

Thus, development of new strategies to replace HF etching is important. A mixture of fluoride salts (e.g., lithium fluoride, LiF) and benign acids (e.g., hydrochloric acid, HCl) is another effective etchant for some MAX phases.[61] After reacting with the in-situ-formed HF of a LiF/HCl solution, Ti_3AlC_2 is converted into accordion-like $Ti_3C_2T_x$, similar to that in traditional HF etching. The resultant $Ti_3C_2T_x$ conductive clay showed strong plasticity that allowed it to be rolled into different shapes (Figure 4A). A freestanding MXene film was then fabricated with excellent flexibility and high conductivity (Figure 4B), which could be directly used as a high-performance electrode for supercapacitors. In addition to the successful etching with better safety, this method has another advantage over traditional HF etching, which is the convenience of delamination. Li-ions can insert and remain in between MXene layers after etching, resulting in an increased interlayer spacing. Thus, MXene nanosheets can be obtained by manual shaking/sonication without extra steps of intercalation. In theory, the interlayer spacing of MXenes can be further regulated by using different fluoride salts, meeting the application requirements of different metal–ion batteries. Among the various combinations

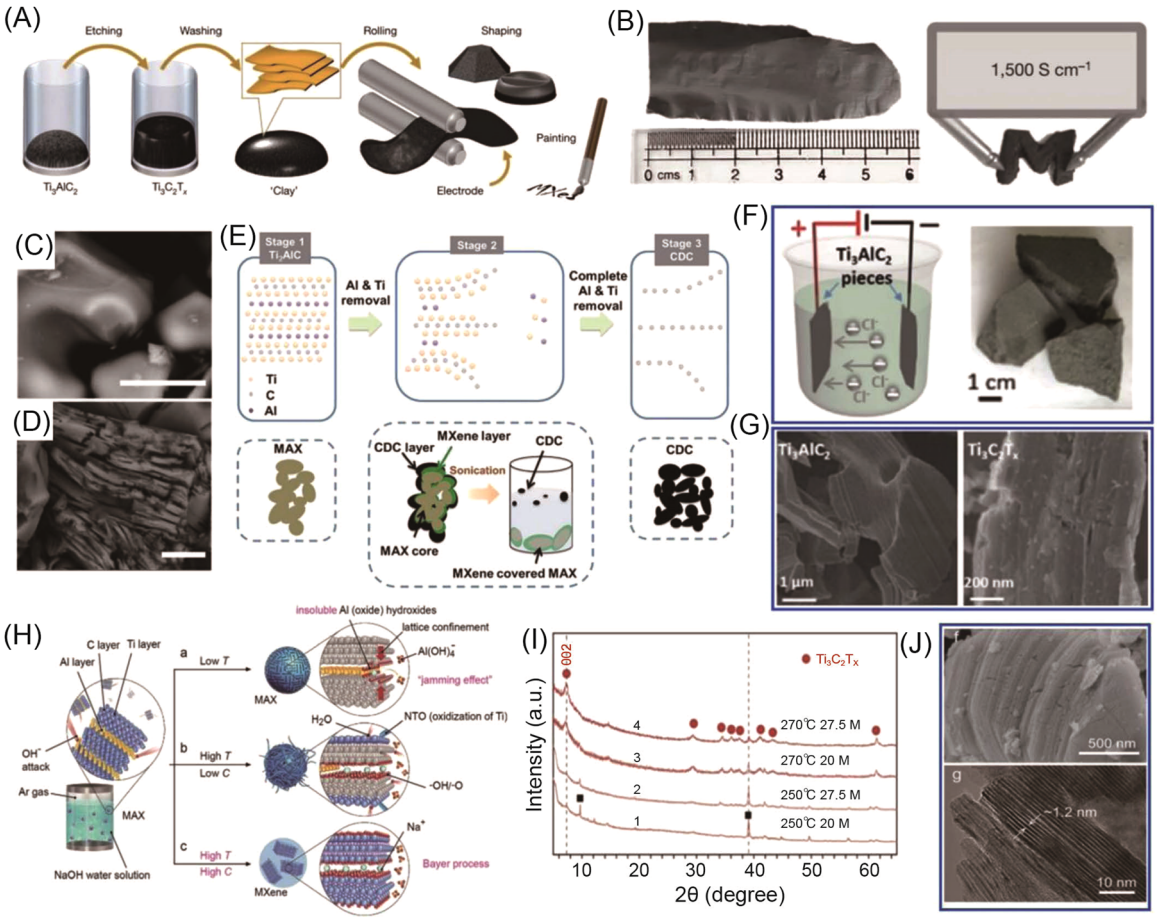

FIGURE 4 (A) The MAX phase is etched in a solution of acid and fluoride salt, and then washed with water till neutral. The resulting sediment behaves like a clay that can be rolled to obtain flexible, freestanding films, or be molded and dried to produce conductive objects with desired shapes. (B) Digital photos showing a freestanding and conductive $Ti_3C_2T_x$ "clay" film. Reproduced with permission: Copyright 2014, Springer Nature.[61] Scanning electron microscope (SEM) images of Ti_2AlC (C) before and (D) after electrochemical etching in 1 M HCl at 0.6 V for 5 days. (E) Proposed mechanism of electrochemical etching of Ti_2AlC in a HCl aqueous electrolyte. Reproduced with permission: Copyright 2017, Royal Society of Chemistry.[62] (F) Configuration of an assembled electrochemical cell using bulk Ti_3AlC_2 as the anode and the cathode in a binary aqueous electrolyte (left), and photo of a Ti_3AlC_2 electrode (right). (G) SEM images of Ti_3AlC_2 before (left) and after (right) electrochemical etching in 1 M ammonium chloride and 0.2 M tetramethylammonium at 5 V. Reproduced with permission: Copyright 2018, Wiley-VCH.[63] (H) Reactions between Ti_3AlC_2 and NaOH water solution under different conditions. (I) X-ray diffraction (XRD) patterns of Ti_3AlC_2 after a hydrothermal treatment using NaOH as an etchant at different temperatures. (J) SEM (top) and transmission electron microscope (bottom) images of $Ti_3C_2T_x$ obtained using 27.5 M NaOH at 270°C. Reproduced with permission: Copyright 2018, Wiley-VCH[64]

of fluoride salts and acids, LiF/HCl is still the most widely used recipe because it can etch and delaminate MAX phases in one step.[50] Besides, there are other fluoride-based etching methods that can avoid direct use of HF. For example, ammonium bifluoride (NH_4HF_2) is able to etch Al layers from Ti_3AlC_2 in water or in propylene carbonate.[65,66] Some molten fluoride salts (e.g., potassium fluoride, KF, and sodium fluoride, NaF) could etch Al from Ti_4AlN_3 at 550°C as well.[47]

At present, the mainstream fluoride etching of MXenes inevitably introduces abundant –F groups and will negatively affect the energy storage performance.[67] Actually, a few F-free etching strategies have been developed in recent years and endowed MXenes with the desired properties.[20,50,59] Electrochemical etching is a good example; it removes Al atomic layers from MAX phases in an F-free electrolyte. Specifically, the working electrode of Ti_2AlC was converted into Ti_2CT_x and carbide-derived carbon at an etching voltage of 0.6 V using a three-electrode system with HCl, Ag/AgCl, and Pt as the electrolyte, reference, and counter electrodes, respectively (Figure 4C,D).[62] The carbide-derived carbon would cover the surface of Ti_2AlC and thus limit etching, resulting in an MXene-covered MAX as indicated in Figure 4E. As for Ti_3AlC_2, F-free electrochemical etching was achieved via using an aqueous electrolyte of 1 M

ammonium chloride and 0.2 M tetramethylammonium in a two-electrode system at 5 V, where bulk Ti_3AlC_2 was used as both the anode and the cathode (Figure 4F,G).[63] In addition, alkali etching methods represent another group of options to avoid fluorine contamination. For example, a hydrothermal treatment of Ti_3AlC_2 using 27.5 M sodium hydroxide (NaOH) at 270°C could realize partial etching of Al atomic layers and produce a mixture of MAX and MXene (Figure 4H–J).[64] Although the above strategies can eliminate –F groups, corrosive chemicals are still needed as indispensable components, resulting in similar safety risks as those that exist in traditional HF etching. Most of the existing etching methods are only effective for Al-based MAX phases, which cannot fully take advantage of the MXene family. Thus, a green etching strategy with better safety and universality is challenging for MXene synthesis. A significant breakthrough was recently achieved using a Lewis acidic molten salt etching method, which has high chemical safety and a wide etching range.[68] Various MXenes could be etched from different MAX phases with A elements of Al, Si, Zn, and Ga using $ZnCl_2$ or $CuCl_2$ as Lewis acidic molten salts in a temperature range of 500–750°C. The uniform surface terminations of –Cl make this etching method even more attractive for battery applications.

Despite the successful etching of different MXenes as shown in Table 1, there is still room for developing etching strategies for MXene synthesis according to the desired properties required by specific applications. For flexible batteries, it is recommended that the etched MXenes have a few features that are important for both flexibility and charge storage, such as large lateral size, few defects, fluorine-free surface, high conductivity, and large interlayer spacing. However, the current etching strategies cannot confer these advantageous features simultaneously, which will possibly lead to unsatisfactory battery performance (e.g., poor rate capability and cycling stability). Thus, continuous development of etching strategies is necessary for the design of high-performance MXene-based flexible batteries.

2.2 | Intercalation and delamination strategies of MXenes

After etching, multilayers of accordion-like MXenes are stacked together by van der Waals and hydrogen bonds. These multilayer MXenes can further transform into single- or few-layer nanosheets via intercalation and delamination. The resultant MXene flakes have the same properties as accordion-like MXenes such as rich surface chemistry, good hydrophilicity and high conductivity, and several distinctive characteristics such as good flexibility and large interlayer spacing. The key to successful delamination is to break the prevailing bonds between the multilayers of MXenes. Few-layer thick MXene flakes could be delaminated with the help of ultrasonication. Nevertheless, the yield is far from satisfactory because the shearing force created by ultrasonication only breaks the strong interactions between MXene layers occasionally. The introduction of intercalators, including organic and inorganic ones, has been proven to be an effective strategy to weaken the interlayer interactions and facilitate delamination (Figure 5A). Thus, various combinations of intercalation and delamination have been developed to synthesize MXene nanosheets since their discovery.

Dimethyl sulfoxide (DMSO) was used as an intercalator to facilitate the delamination of multilayer $Ti_3C_2T_x$.[89] After intercalation of DMSO molecules, the interlayer spacing of

TABLE 1 Representative etching of different MXenes

Method classification	MXene types	Etchant	References
Hydrofluoric acid (HF) etching	$Ti_3C_2T_x$, V_2CT_x, Ti_2CT_x, Nb_2CT_x, Mo_2CT_x, Ti_2NT_x, Ti_3CNT_x, $Mo_2TiC_2T_x$, $Mo_2Ti_2C_3T_x$, $V_4C_3T_x$, $Nb_4C_3T_x$, $Zr_3C_2T_x$, and so forth	HF, HF + HCl	[14,69–81]
In situ-formed HF etching	$Ti_3C_2T_x$, V_2CT_x, Nb_2CT_x, Mo_2CT_x, Ti_2CT_x, Ti_3CNT_x, $Cr_2TiC_2T_x$, $W_{1.33}CT_x$, and so forth	Acid: HCl, H_2SO_4 Salt: LiF, NaF, KF, NH_4F, CsF, CaF_2, and so forth	[31,48,57,61,82–86]
	$Ti_3C_2T_x$	NH_4HF_2, NH_4F	[65,87]
Alkali etching	$Ti_3C_2T_x$	NaOH	[64]
Electrochemical etching	Ti_2CT_x, $Ti_3C_2T_x$	HCl, NH_4Cl + TMAOH	[62,63]
Molten salt etching	$Ti_4N_3T_x$	KF + LiF + NaF	[47]
	$Ti_3C_2T_x$, Ti_3CNT_x, Nb_2CT_x, Ta_2CT_x, Ti_2CT_x, and so forth	$ZnCl_2$, $CuCl_2$, $NiCl_2$, $FeCl_2$, AgCl, $CoCl_2$, $CdCl_2$, $CdBr_2$, and so forth	[20,68,88]

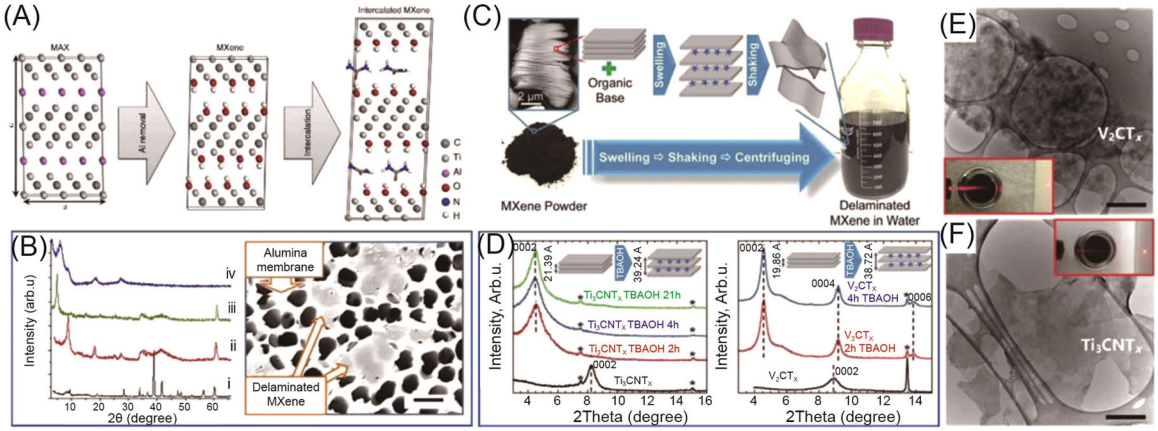

FIGURE 5 (A) Schematic of the synthesis and intercalation of $Ti_3C_2T_x$. (B) X-ray diffraction (XRD) patterns of (i) Ti_3AlC_2, (ii) exfoliated, (iii) dimethyl sulfoxide intercalated, and (iv) delaminated $Ti_3C_2T_x$ (left); scanning electron microscope image of delaminated $Ti_3C_2T_x$ on an alumina membrane (right). Reproduced with permission: Copyright 2013, Springer Nature.[89] (C) Schematic of the MXene delamination process using an organic base. (D) XRD patterns of Ti_3CNT_x before and after mixing with tetrabutylammonium hydroxide (TBAOH) for 2, 4, and 21 h (left). XRD patterns of V_2CT_x before and after mixing with TBAOH for 2 and 4 h (right). TEM images of (E) a delaminated V_2CT_x nanosheet and (F) a delaminated Ti_3CNT_x nanosheet. Insets show the Tyndall effect for V_2CT_x and Ti_3CNT_x aqueous solution, respectively. Reproduced with permission: Copyright 2015, Royal Society of Chemistry[90]

multilayer $Ti_3C_2T_x$ was enlarged as proven by the change of the corresponding XRD patterns (Figure 5B). Thus, the strong interactions between $Ti_3C_2T_x$ layers were reduced significantly. Single- or few-layer $Ti_3C_2T_x$ would then be delaminated by simple ultrasonication as expected (Figure 5B). These $Ti_3C_2T_x$ nanosheets can further assemble into a freestanding film with a large interplanar spacing via filtration, applicable for flexible energy storage devices. In addition to DMSO, some other organic solvents have also been used as intercalators for delaminating multilayer $Ti_3C_2T_x$, for example, urea and *N*,*N*-dimethylformamide. However, the yield of delaminated $Ti_3C_2T_x$ nanosheets is not high enough even after the intercalation of DMSO and its relatives. Moreover, DMSO has shown ineffective intercalations toward the delamination of some other MXenes (e.g., V_2CT_x and Mo_2CT_x).[50] A group of organic alkali with relatively large molecule structures (e.g., tetrabutylammonium hydroxide, TBAOH, and *n*-butylamine) have been proven to have better efficiency of intercalation for various MXenes (Figure 5C).[90] After the dissociation of organic alkali in the aqueous solution of multilayer MXenes, alkali cations would intercalate in MXene layers and widen their interlayer space significantly (Figure 5D). As a result, multilayer MXenes could be delaminated by mild ultrasonication or manual shaking. In addition to $Ti_3C_2T_x$, single-layer Ti_3CNT_x and V_2CT_x nanosheets were obtained using the above intercalation strategy (Figure 5E,F). The use of organic alkali can reduce –F group concentrations and increase the oxygen content of MXene nanosheets,[50,90] which is useful for the battery application.

In addition to screening intercalators, the optimization of intercalation methods is another aspect that deserves special attention as it can cause ideal delamination of multilayer MXenes. As suggested by a representative work, the remaining Ti–Ti and/or Ti–Al bonds between $Ti_3C_2T_x$ layers will inhibit the effective diffusion of intercalators because of their higher bonding strength.[53] Therefore, the delamination yield of MXene nanosheets in traditional synthesis is low even under strong ultrasonication.

To improve intercalator diffusion, a hydrothermal-assisted intercalation strategy (HAI) was introduced with tetramethylammonium hydroxide (TMAOH) and ascorbic acid as an intercalator and a reductant, respectively (Figure 6A). Under high temperatures and high pressures, TMAOH could effectively intercalate into $Ti_3C_2T_x$ multilayers, which facilitates the subsequent delamination (Figure 6A). The yield of $Ti_3C_2T_x$ nanosheets reached 74% via the HAI process, as shown in Figure 6B,C.[53] Similarly, a microwave treatment was used to facilitate the intercalation of TMAOH and the subsequent delamination of multilayer MXenes. However, the yield of $Ti_3C_2T_x$ nanosheets based on this strategy was relatively low.[91] Previous research has suggested that the coexistence of water and oxygen, especially at high temperatures, will make MXene nanosheets unstable.[92,93] Thus, during the intercalation, many defects would be generated on MXene nanosheets, resulting in poor stability and a relatively low conductivity.[53,94] Moreover, the long-term hydrothermal treatment and ultrasonication would also lead to a decrease of

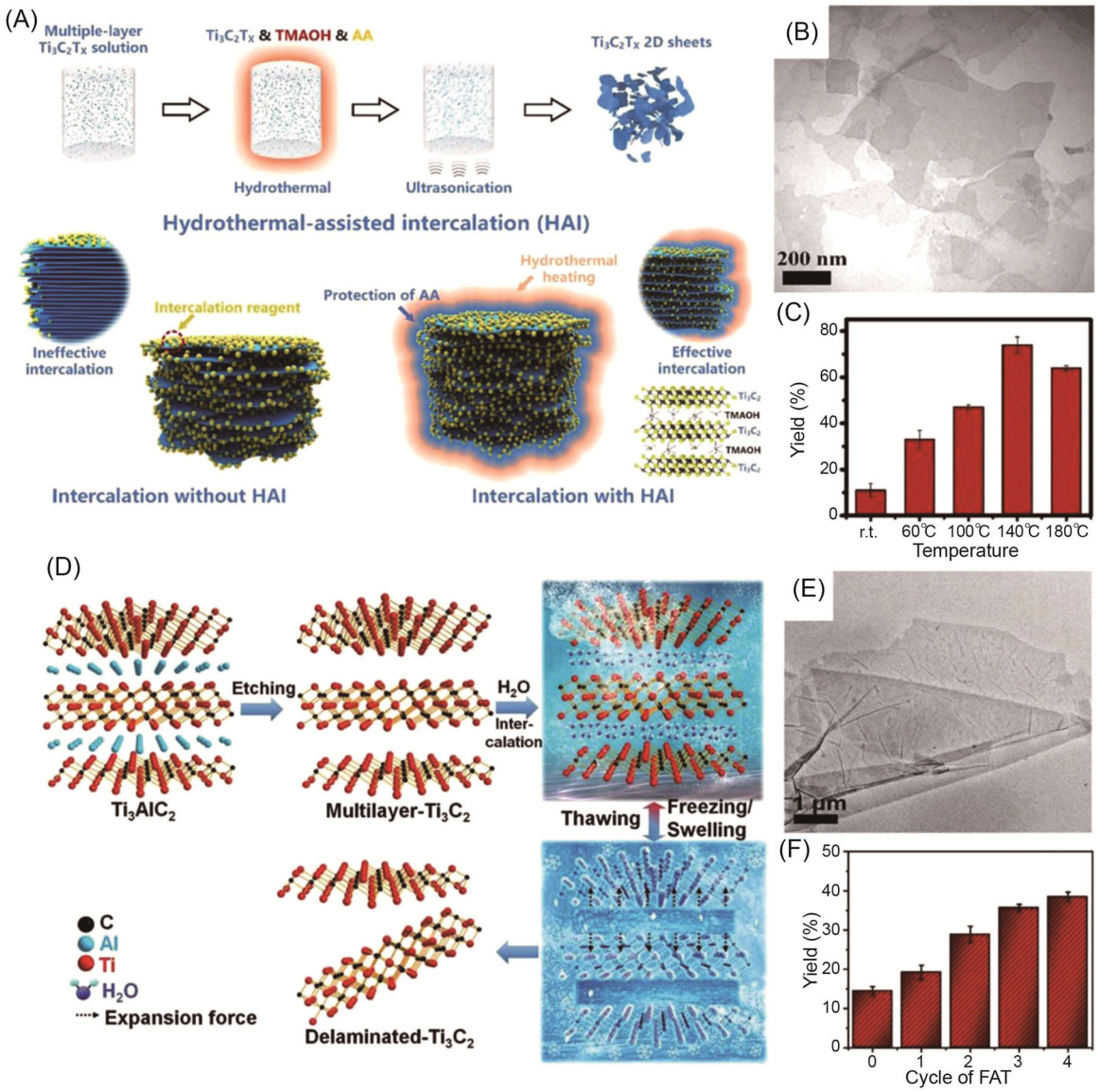

FIGURE 6 (A) Schematic of the hydrothermal-assisted intercalation (HAI) strategy to synthesize $Ti_3C_2T_x$ nanosheets. (B) Transmission electron microscope (TEM) image of $Ti_3C_2T_x$ nanosheets obtained using the HAI strategy. (C) Comparison of yields at various temperatures using the HAI strategy. Reproduced with permission: Copyright 2019, American Chemical Society.[53] (D) Schematic of the freeze-and-thaw (FAT) method to synthesize $Ti_3C_2T_x$ nanosheets. (E) TEM image of $Ti_3C_2T_x$ nanosheets obtained using the FAT method. (F) Comparison of yields at different cycle times of FAT. Reproduced with permission: Copyright 2020, Wiley-VCH[54]

lateral sizes of MXene nanosheets. To solve the above-mentioned problems, a freeze-and-thaw (FAT)-assisted method was proposed to cleave MXene nanosheets from multilayer MXenes based on the expansion force of water-freezing (Figure 6D).[54] After repeated freezing and thawing, the interlayer spacing between adjacent $Ti_3C_2T_x$ layers was enlarged significantly, and a lot of $Ti_3C_2T_x$ nanosheets, therefore, separated from multilayer $Ti_3C_2T_x$ spontaneously, as shown in Figure 5E. The yield of large $Ti_3C_2T_x$ nanosheets reached 39% without ultrasonication after four cycles of the FAT process (Figure 6F). When 1 h ultrasonication was further applied, the yield of $Ti_3C_2T_x$ nanosheets increased to 81.4%, but the lateral size of $Ti_3C_2T_x$ nanosheets reduced inevitably. Due to the mild conditions of their synthesis, the $Ti_3C_2T_x$ nanosheets obtained by the FAT method showed both high conductivity and high mechanical strength,[54] which could be readily used for flexible energy storage devices.

The major challenge of MXene synthesis is still related to etching rather than intercalation and delamination. These flexible and conductive MXene nanosheets can homogeneously disperse in a variety of solutions,[95,96] and assemble into freestanding films,[35,97]

flexible fibers,[98,99] compressible sponges,[100,101] and vertical arrays.[102,103] MXene flakes have additional functionalities, for example, superconductivity, by making good use of their surface chemistry.

3 | FLEXIBLE MXENE FILMS FOR ENERGY STORAGE DEVICES

MXene flakes dispersed in solutions can be easily fabricated into films by coating, printing, and vacuum filtration. MXene films possess a couple of advantages, including high electrical conductivity and mechanical robustness. The high electrical conductivity allows for the construction of nanoscale circuitry in MXene films, which facilitates the electron-transfer process. As the rate capability (C) is inversely proportional to the square of the diffusion length (L; $C = \alpha D/L^2$, where α is a constant and D is the diffusivity), the inter-flake and interlayer spaces capable of accommodating ions are charge-transfer sites with a small L value and high electrical conductivity. Notably, the charge storage mechanisms are related mainly to the inherent properties of MXene, such as interlayer distances, distances between MXene walls, and surface functional groups. Therefore, the discussion on the energy storage performance of flexible MXene films focuses on film structures and surface chemistries.

3.1 | Structural impacts on energy storage

Restacking of MXene flakes will diminish the advantages of high electrical conductivity and short diffusion length to charge-transfer sites. Intuitively, addition of spacers, such as nanotubes and intercalation nanocrystals, can alleviate the restacking to a limited extent.[29,33,104,105] The original layered structure is disrupted by spacers, resulting in tortuous paths for ion transport. Besides, the spacer materials are often inactive in energy storage, thus reducing the specific capacity (volumetric and gravimetric) of MXene films. It is critical to control the number of spacers added. As expected, in most cases, the volumetric capacitances of MXene hybrid films are lower than those for pure MXene films. For instance, at a low rate ($<100\ \mathrm{W\ kg^{-1}}$ or $<300\ \mathrm{W\ L^{-1}}$), the gravimetric or volumetric capacitance of an MXene hybrid film containing 5 wt% graphene is lower than that for a pure MXene film (Figure 7A,B).[104] For other spacer nanomaterials, NbN nanocrystals, for instance, the volume capacity increased only at 0.5 wt% of the additions in the range from 0.33 to 0.8 wt% (Figure 7C,D).[105]

Alternatively, creation of holes on MXene flakes can improve the ion diffusion in the vertical direction. Thanks to the redox activity of MXene, porous structures can be created by the oxidation of MXene flakes. Oxygen-terminated titanium atoms can be removed during the anodic oxidation, forming titanium oxides. Meanwhile, carbon atoms previously connected to titanium would be exposed and bond with adjacent exposed carbon atoms. As a result, the ordered structure is interrupted, producing a porous structure. Excessive oxidation will entirely transform MXene into amorphous carbon and titanium oxides, losing the energy storage ability. Therefore, precise control of the degree of oxidation is important. For example, the energy density gradually increases with more anodic oxidation cycles at 0.1 V. At a higher oxidation potential, the energy density and power density decrease dramatically because MXene flakes are destroyed (Figure 8A,B).[106] The same concept can be introduced for the synthesis of the MXene film. Concentrated sulfuric acid is used for partial oxidation of MXene flakes. With reduced lateral sizes and nanoporous structures, the gravimetric capacitance increases by more than five times at a high scan rate (Figure 8C,D).[107] To achieve a scalable synthesis of MXene films, oxidation during the film formation is better than electrochemical oxidation.

Another way to bypass the restacking issue is to vertically align them during the formation of a film. MXene flakes dispersed in an aqueous solution can form discotic liquid crystal phases, among which discotic smectic and columnar phases can be aligned in 1D and 2D lattices, respectively. To do so, the MXene flakes are controlled to approximately 219 ± 47 nm in lateral dimension and around 6 μm in thickness (Figure 9A).[103] When dispersed in water, MXene flakes can automatically be aligned vertically. However, the alignment becomes more challenging with an increase in thickness because the surface-anchoring effect decreases dramatically. The mechanical shearing force effectively addresses this problem, but the polydispersity in the shape and size of MXene flakes still imposes challenges. Hexaethylene glycol monododecyl ether, as a surfactant, is able to enhance the interactions between MXene flakes, thus facilitating the vertical alignment under the mechanical shearing force. The vertically aligned MXene film shows a thickness-independent redox behavior as the thickness increases from 40 to 200 μm. Negligible distortion in cyclic voltammetry curves is observed at a rate of up to $1000\ \mathrm{mV\ s^{-1}}$, demonstrating excellent rate capability. However, the independence on the film thickness is still limited, and the rate capability declines when the thickness exceeds 200 μm. A thick film (320 μm) still shows a sharp drop in capacitance at a scan rate higher than $100\ \mathrm{mV\ s^{-1}}$ (Figure 9B).

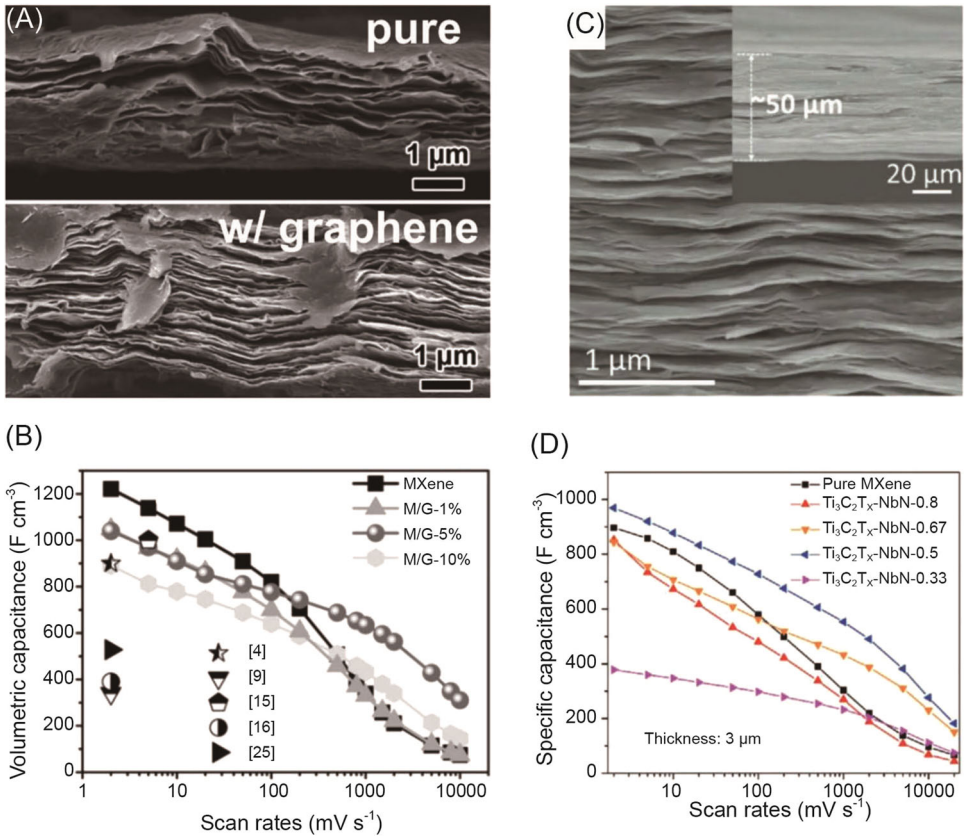

FIGURE 7 (A) Scanning electron microscope (SEM) images of the cross-section and (B) volumetric capacitance of MXene films with and without graphene as spacers. Reproduced with permission: Copyright 2017, Wiley-VCH.[104] (C) SEM images of the cross-section of an MXene film with NbN as the spacer and (D) volumetric capacitance with and without NbN as spacers. Reproduced with permission: Copyright 2020, Wiley-VCH[105]

Most of the above methods to prevent restacking of MXene flakes are used for supercapacitors. For batteries, it is also necessary to consider the restacking problem and apply similar strategies to improve the energy storage performance.

3.2 | Surface chemistry for energy storage

MXenes are good negative electrodes (anodes) for various energy storage devices. In general, the electrical double-layer (EDL) model applies to the MXene flakes in aqueous solutions (Figure 10A).[24] The hybridization of atomic orbitals of cations with the MXene orbitals is interrupted by the solvation shell. As a result, an inner potential difference is established upon the intercalation of hydrated cations and water molecules, forming an EDL within the interlayer spaces in MXene flakes. The EDL capacitance is expressed as $C = \varepsilon_r \varepsilon_0 A/(b - a)$, where ε_r is the dielectric constant between MXene and cations, ε_0 is the vacuum permittivity, A is the surface area, b is the distance between MXene walls, and a is the ionic radius. This equation also demonstrates the importance of MXene synthesis in producing an optimal design to achieve a minimal value of $(b - a)$. The exposed titanium is slightly reduced along with the electron storage, though the extent is too small (i.e., 0.05 e^- and 0.05 Li^+ per titanium atom in a 1 M Li_2SO_4 electrolyte) to contribute a significant amount to the pseudocapacitance. However, Faradaic reactions will occur between protons and metal–oxygen bonds in a strong acidic electrolyte, thus increasing the Faradaic contributions in energy storage. As expected, broad redox peaks are often observed for MXene-based supercapacitors using sulfuric acid as the electrolyte.

Batteries often use nonaqueous electrolytes because alkali metals can react with water. In nonaqueous electrolytes, cations can be partially desolvated, and their atomic orbitals are able to hybridize with MXene orbitals, especially for the surface termination groups

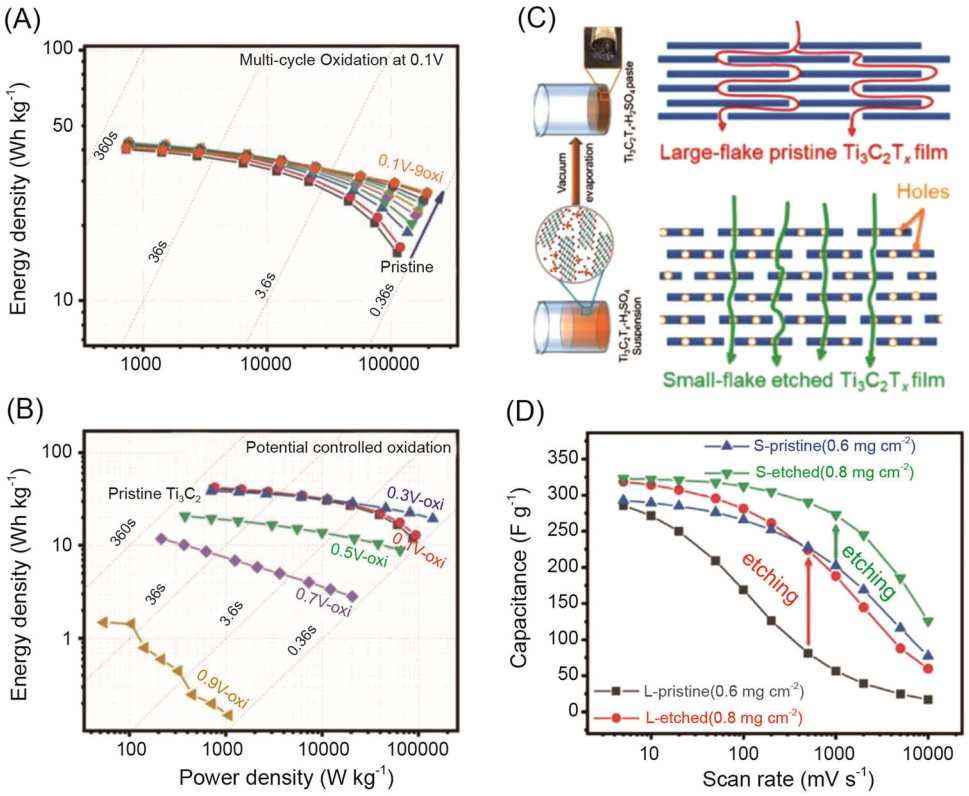

FIGURE 8 Energy density comparison of electrochemical oxidation of MXene with (A) different cycles and (B) various voltages. Reproduced with permission: Copyright 2019, Wiley-VCH.[106] (C) Schematic illustration of oxidization of MXene by sulfuric acid and (D) capacitance with different sizes. Reproduced with permission: Copyright 2020, Wiley-VCH[107]

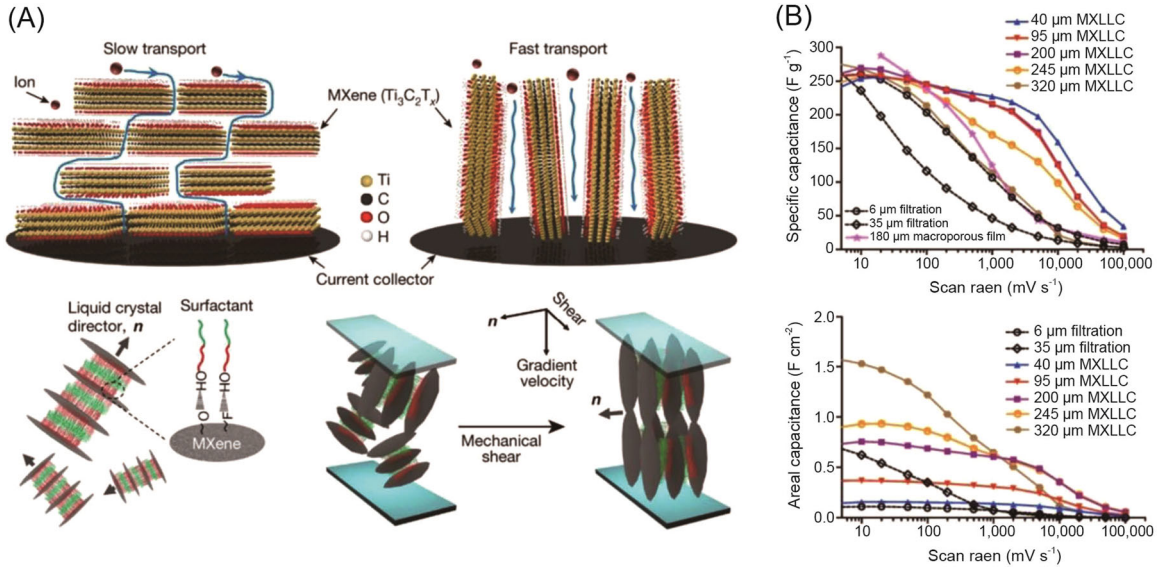

FIGURE 9 (A) Ion transport in MXene films and alignment under mechanical shearing force. (B) Gravimetric and area capacitance of the vertically aligned MXene and their dependence on thickness. Reproduced with permission: Copyright 2018, Springer Nature[103]

(Figure 10B). As a result, MXene can be reduced, and its charge storage mainly arises from the pseudocapacitance (Figure 10C).[24] In the context of orbital hybridization, it is important to choose proper cations and surface termination groups of MXene flakes, which are closely related to the synthesis of MXene. Several recent reviews have well summarized the developments of MXene for batteries.[25,108–112] Unlike common battery chemistry,

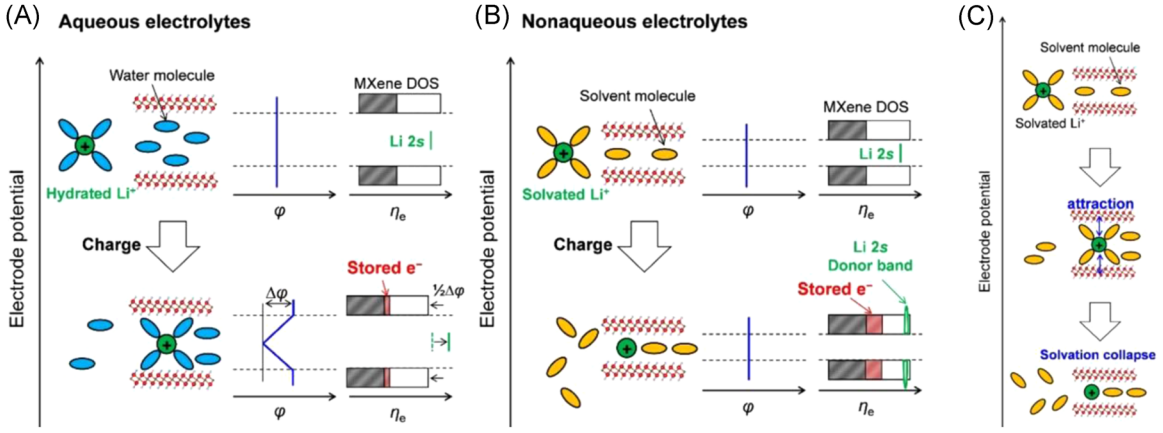

FIGURE 10 Schematic illustrations of structural changes and changes in the electronic structure of MXene in (A) aqueous and (B) nonaqueous electrolytes and (C) during the initial stage of charge. Reproduced with permission: Copyright 2018, American Chemical Society[24]

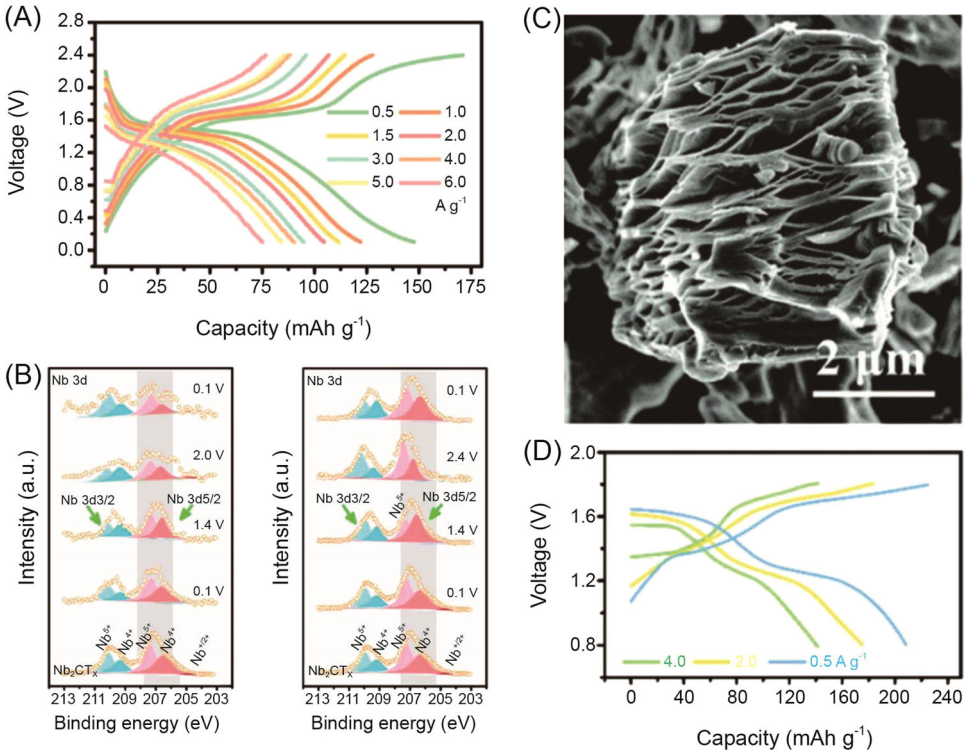

FIGURE 11 (A) Charge/discharge plateaus of Nb_2CT_x MXene at various current densities and (B) reduction of Nb with excessive oxidation indicated by X-ray photoelectron spectroscopy spectra. Reproduced with permission: Copyright 2021, Elsevier.[113] (C) Scanning electron microscope image and (D) charge/discharge profiles of halogenated MXene. Reproduced with permission: Copyright 2020, Royal Society of Chemistry[114]

pseudocapacitance indicates no discharge/charge voltage plateaus, increasing the difficulty of providing a stable discharge power.

Recently, the Nb_2CT_x MXene showed a pair of charge/discharge plateaus due to the extensive reduction of Nb by deep intercalation of zinc ions (Figure 11A,B).[113] The critical factor in obtaining such results is expanding the voltage window to 2.4 V, far beyond the typical stable voltage window of water (1.23 V). To do so, a water-in-salt electrolyte (21 M LiTFSI and 1 M $Zn(OTf)_2$) was used to prevent the water electrolysis. This pioneering work offers a promising result for MXenes as intercalation-type electrode materials for energy storage devices. Considerable efforts are required to explore a similar property for

other materials of the MXene family. Precise synthesis of diverse MXenes and manufacture of MXene electrodes are prerequisites for the exploration. Moreover, the deep intercalation process in nonaqueous electrolytes needs further investigation.

Taking advantage of the redox activity of MXene stemming from its abundant surface termination groups, MXene can act as a host for redox reaction-based energy storage. Sulfur can be easily loaded onto MXene flakes by placing MXene in melted sulfur or through a hydrothermal reaction with sulfides.[115] These simple strategies have been able to show the advantages that MXene confers, namely, the high electrical conductivity of the MXene core and the strong binding of the sulfur species to the surface termination groups. Chemical modifications can further improve the performance of MXene flakes as a host. For example, on doping with heteroatoms (e.g., nitrogen and metal atoms), MXene flakes can catalyze the redox reaction by the strong interaction between lithium polysulfides and heteroatoms.[116] For example, MXene implanted with Zn atoms could host a high loading of sulfur (89 wt%) and deliver a high capacity of 1136 mAh g^{-1} at 0.2 C. More importantly, the capacity retained is more than 500 mAh g^{-1} at a high rate of 6 C. Despite these advantages, the stress induced by the reversible sulfur reaction may cause the collapse of MXene flakes and, therefore, battery failure.

Abundant surface termination groups of MXene provide additional possibilities. Iodine atoms are able to bond to −F, −O, and −OH functional groups. In particular, the binding energy of iodine atoms to −OH functional groups is as low as −3.68 eV.[117] As a result, the MXene flakes are used as an interface layer in a lithium–iodine battery, which acts as a host for iodine species that prevent the shuttle effect. In this case, iodine-doped graphene was used as the cathode to provide iodine. Recently, MXene was halogenated by a molten salt etching process. For example, the Ti_3AlC_2 precursor was etched by molten CuI_2, producing $Ti_3C_2I_2$ flakes (Figure 11C).[114] The halogenated MXene was directly used as the cathode in a zinc–metal battery with $ZnCl_2$ and KCl as the electrolyte. The Cl^- ions facilitated the redox reaction of I^0/I^+. As a result, intensive redox reactions are involved in energy storage, thus showing two charge/discharge plateaus (Figure 11D). Following this principle, other reactions involving liquid–solid conversion and oxygen-containing functional groups may also possibly occur at the surface of MXene flakes.[118] The redox-flow battery is based on exactly the above principle. Therefore, this type of battery would be possible to provide more ideas to extend the MXene use in batteries, cathode component for instance.[119]

In short, Table 2 presents a brief overview of the surface chemistry of MXenes for batteries. It is noteworthy that this table does not provide a comprehensive account of diverse batteries because frequently updated review articles about MXenes for energy storage technologies have already provided such information.[25,26,109,110] Instead, we present a general prediction on the effects of functional groups of MXenes on metal–ion diffusion, which would hopefully provide a brief guidance for the synthesis of MXenes for high-performance energy storage. In addition, we summarize the prototypes of modifying surface terminations on MXenes to utilize energy storage mechanisms beyond metal–ion intercalation, which may also represent a direction to achieve energy-dense storage based on MXenes.

4 | MXENE FILMS FOR SENSORS

Flexible sensors are core components for flexible electronics.[121] They are able to transduce temperature, light, pressure, mechanical strain/stress, and chemical concentrations to readable electrical signals. MXene films are fabricated by interconnecting small flakes, forming a conductive network. Under mechanical strain/stress, the overall resistance changes because the interconnects of flakes may be disrupted. Using this property, MXene films can be used as strain/stress sensors, which have a wide range of applications from robotics to wearable healthcare diagnosis. To act as a

TABLE 2 Brief overview of the surface chemistry of MXenes for batteries

Functional groups/surface terminations	Stacking mode	Metal–ion diffusion	References
OHO	Intercalation in triangular stacking	Fast	[120]
OO	Intercalation in octahedral stacking	Slow	
S	Conversion reaction	-	[113]
I_2	Conversion reaction	-	[115,116]
Nb	Intercalation	-	[114]

strain/stress senor, MXene films should preferably be stretchable. As such, stretchable polymers such as rubber, polyurethane, and hydrogels are often composited with MXene flakes.[121] The sensitivity of strain/stress sensors is characterized by the gauge factor (the ratio of resistance changes to strain). The sensitivity of MXene films can even reach more than 10,000. For instance, a composite consisting of MXene and polyurethane shows a gauge factor of 128,800 (Figure 12A,B).[122] The same mechanism applies to mechanical compression. Conductive networks with MXene flakes will change and, therefore, the resistance will vary. Besides, highly conductive MXenes can act as current collectors to sense the contact resistance. For instance, interdigital electrodes coated by MXene are patterned on a flexible substrate, and a polydimethylsiloxane layer is layered onto the interdigital electrodes. The sensitivity can reach up to 33.8 kPa^{-1} (Figure 12C,D).[123]

Another characteristic of MXenes is their abundant surface termination groups, by which chemical modifications on the surface can be precisely translated into electrical signals. Oxygen-terminated Ti_2C MXene shows semiconductor behavior and selective absorption of ammonia gas.[124] Upon absorption, a charge transfer occurs, thus generating electrical signals. $Ti_3C_2T_x$ MXene flakes were coated on a flexible polyimide substrate and demonstrated good sensitivity of vapors including acetone, ethanol, methanol, and ammonia.[125] Water molecules can also be absorbed on the MXene surface with functional groups by establishing hydrogen bonds. The absorbed water molecules are stabilized at the surface in the form of hydronium ions, which alter the conductivity of MXene flakes. For instance, $Ti_3C_2T_x$ MXene showed a high conductivity of 243 Ω in dry air and markedly increased to more than 6000 Ω at high humidity (relative humidity = 80 ± 5%).[126] Water molecules can gradually oxidize MXene flakes, especially $Ti_3C_2T_x$ MXene, to metal oxides, resulting in sensor failure. Protective layers are grown on the surface to prevent unwanted oxidation.[127]

The electrochemical activity of MXene flakes allows for the detection of biomarkers. Printed $Ti_3C_2T_x$ MXene was used to detect isoniazid and acetaminophen, two common liver damage drugs. The limit of detection can be lowered down to 0.048 μM in the detectable range of 0.25–2000 μM.[128] Moreover, mycotoxin can be detected in the range of 5 pM–10 nM due to the coordination between surface termination groups and tetrahedral DNA nanostructures.[129]

5 | MXENE FILMS FOR TRANSISTORS

Sensors are the data collection modules in a complete system. Transistors are essential components for processing the collected data. As discussed above, surface termination groups can alter the work function of MXenes. For instance, the work function of the $Ti_3C_2T_x$ MXene is tunable in a range of 1.8–6.2 eV,[46] facilitating its utilization as an electrode material for field-effect transistors. A biologically compatible field-

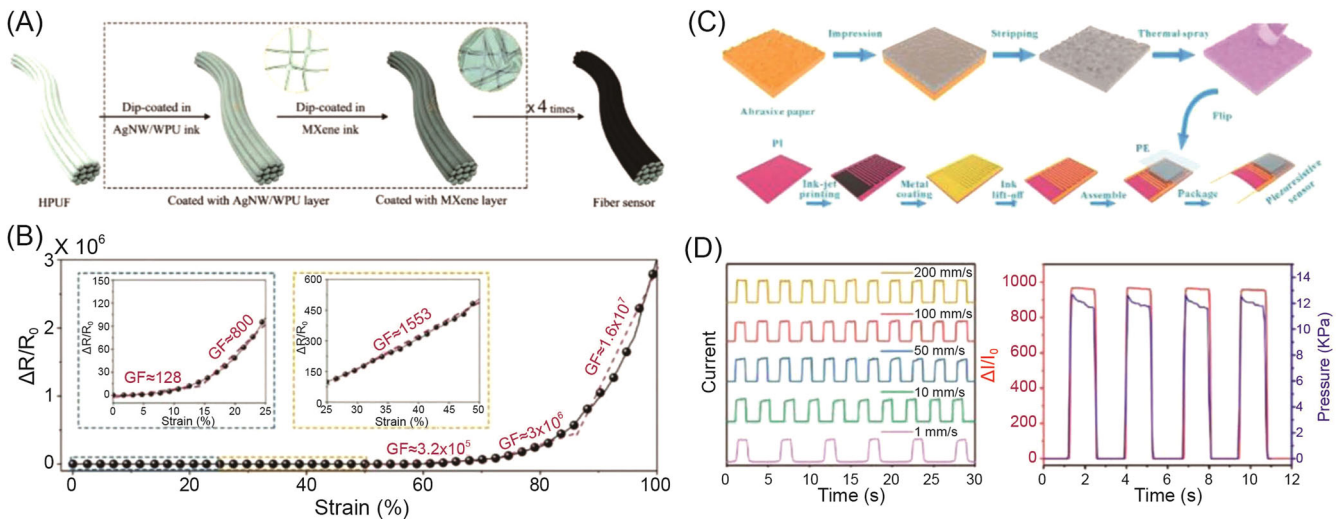

FIGURE 12 (A) Schematic illustration of the fabrication of an MXene composited with waterborne polyurethane as a strain sensor and (B) its sensitivity. Reproduced with permission: Copyright 2019, Royal Society of Chemistry.[122] (C) Schematic illustration of the fabrication of an MXene pressure sensor on a flexible substrate and (D) its sensing performance. Reproduced with permission: Copyright 2020, American Chemical Society[123]

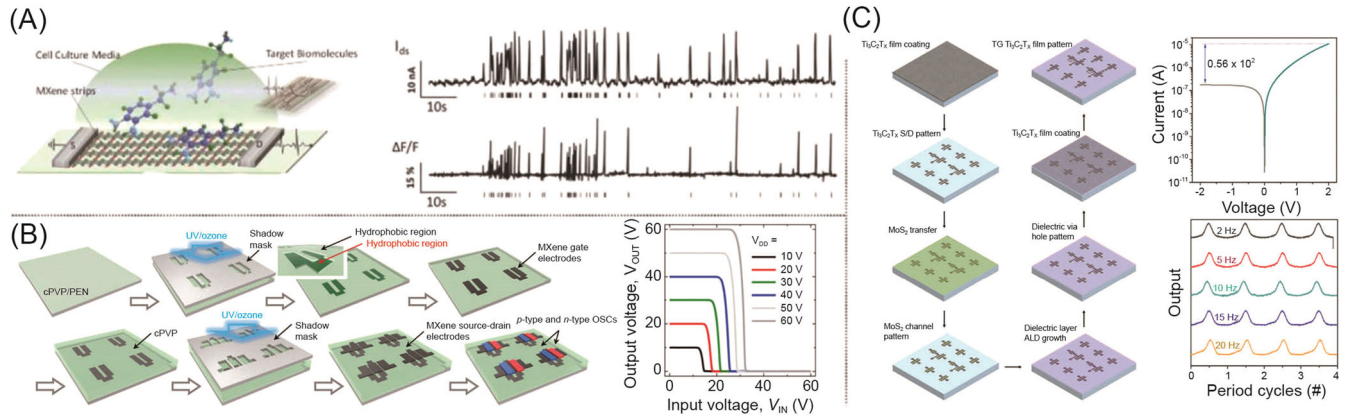

FIGURE 13 (A) Schematic illustration of a field-effect transistor with MXene stripes and its neurosensing ability. Reproduced with permission: Copyright 2016, Wiley-VCH.[130] (B) Schematic illustration of an organic field-effect transistor with MXene as Ohmic contact and its performance. Reproduced with permission: Copyright 2019, American Chemical Society.[131] (C) Schematic illustration of a field-effect transistor with MXene as Ohmic contact and its performance as a rectifier. Reproduced with permission: Copyright 2021, Wiley-VCH[132]

effect transistor was developed by patterning a $Ti_3C_2T_x$ MXene into microstripes on a chip (Figure 13A).[130] A pair of silver electrodes was deposited onto stripes and a solution-gated device was set up. The conductance between the source and the drain electrode was dependent on the gate voltages. The MXene-based device acted as an n-type field-effect transistor when the gate voltage was higher than +0.3 V, whereas it became a p-type field-effect transistor when the gate voltage was decreased to below +0.3 V. This field transistor was used to detect dopamine, a typical neurotransmitter for brain functions, thus demonstrating the possibility of its use in neuromorphic computing applications. MXenes with tunable work functions are also used for building Ohmic contact to improve the carrier injection efficiency.[133–136] Large-scale patterning for scalable applications has been demonstrated. Organic field-effect transistors were fabricated using a dip-coating method (Figure 13B).[131] To pattern MXene films in a parallel fashion, a selective-wetting surface was created by making specific surfaces hydrophilic through UV/ozone treatment that introduces hydroxyl groups on the surface. As MXenes have good hydrophilicity due to their surface termination groups, MXene flakes were only coated to the hydrophilic surface. The MXene film was used as the source, drain, and gate electrodes for organic field-effect transistors, showing excellent device performance. It is also possible to create circuits by combining MXenes and semiconductor materials. A $Ti_3C_2T_x$ MXene film was spray-coated onto a glass substrate and patterned by standard lithography (Figure 13C).[132] This pioneering work demonstrates the possibility to successfully introduce MXenes into microfabrication processes, which is generally difficult for new materials. Deposited MoS_2 layers were used as gates. The parallel manufacture of field-effect transistors showed a good yield of ~96% with narrow variations in device performance. More importantly, the field-effect transistors are integrable into circuits.

6 | MXENE FILMS FOR ANTENNAS

Wireless communication through antennas is the basis for electronics transmitting data and working together. Metals are widely used as antennas due to their high electrical conductivity. However, it is challenging to create thin and flexible metal antennas because their thickness is often thicker than the predicted skin depth depending on frequency. Alternatively, MXene films have shown high electrical conductivity of up to 10,000 S cm^{-1}, making them an excellent candidate for antennas used in radiofrequency communication applications. MXene films were fabricated by spraying MXene ink onto a hydrophilic substrate (Figure 14A).[137] The sheet resistance of a 1.4-μm film was $0.77 \pm 0.08\ \Omega^{-2}$. The MXene antenna showed a gain of up to 1.7 dB. With an increased thickness (8 μm), the antenna had a reflection coefficient of −65 dB at 2.4 GHz. MXene films were then used in a radio frequency identification tag, showing a reading range of almost 8 m when maximum matching is achieved (Figure 14B). Micrometer-thin and flexible Microstrip patch antennas based on MXene were developed recently to replace conventional metals, which is considered to expand the applications to flexible, miniaturized, and wearable devices. With a thickness of 5.5 μm, the radiation efficiency reached more than 99% (Figure 14C).[138]

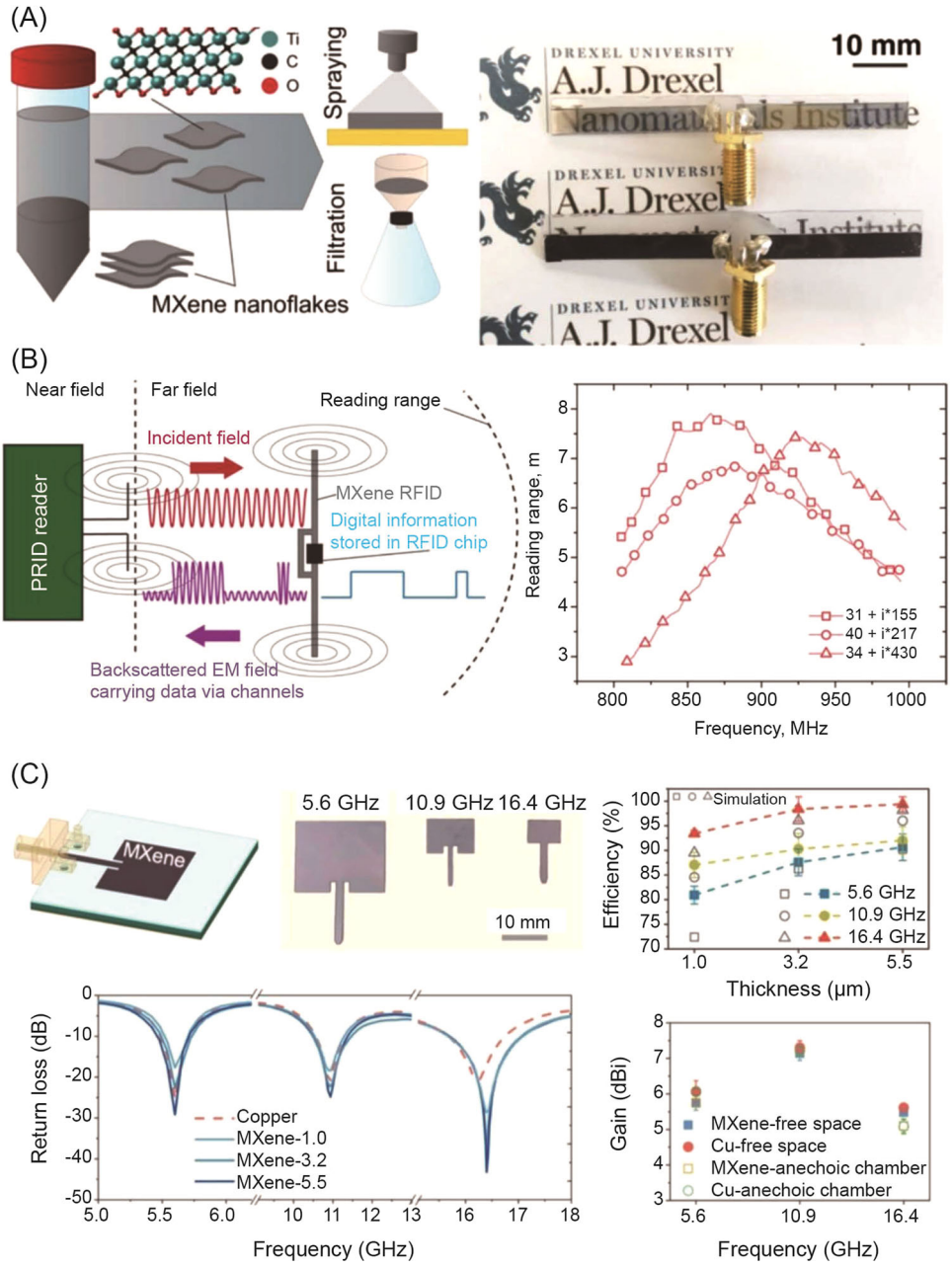

FIGURE 14 (A) Fabrication of MXene film antennas and (B) their use in radio frequency identification. Reproduced under the terms of the CC BY-NC license: Copyright 2018, American Association for the Advancement of Science (AAAS).[137] (C) Return loss and radiation efficiency of MXene patch antennas. Reproduced with permission: Copyright 2020, Wiley-VCH[138]

The efficiency decreased slightly to about 83% when operating at a frequency of 28 GHz. Overall, target frequencies of 5.6, 10.9, 16.4, and 28 GHz were realized by MXene microstrip antennas, proving their potential for use for new 5G communication standards (i.e., sub-6 and 28 GHz).

Due to their outstanding performance in energy storage, MXene films can cover almost all operations of electronics: data collection, processing, and transmission, and act as the power source to drive all these functions.

7 | SUMMARY AND OUTLOOK

MXenes have been widely used in various batteries due to their distinctive advantages in charge storage, such as high conductivity, rich surface chemistry, good hydrophilicity, and large surface area and interlayer spacing. Moreover, MXene films with great flexibility and high mechanical strength guarantee stable electromechanical performance under different deformations. Therefore, many MXene-based flexible batteries have been successfully developed,

some of which provide excllent performance (e.g., high capacity) even after bending, twisting, and stretching. Although some significant achievements have been made, there are still several unsolved problems in terms of MXene-based flexible batteries, ranging from the synthesis of MXenes to the device design of batteries.

It is generally accepted that MXenes can realize pseudocapacitive charge storage with a fast speed via their metal oxide-like surface and transition metal core layers theoretically.[139] This advantage is a major motivation for the application of MXenes in batteries. However, as discussed above, there are deficiencies and limitations in the current synthesis of MXenes, degrading the energy storage capability of MXenes to a large degree. For example, the mainstream fluoride etching of MXenes is effective, but it causes contamination with –F groups, which is one cause for the reduction in conductivity and battery performance. Fluoride-free etching can be an ideal substitution that confers MXenes with better conductivity, but the low yield of MXene flakes is not favorable for practical applications. As such, there is still room for improvements in MXene synthesis that can take advantage of the structural advantages of MXenes in flexible batteries. In particular, green synthesis with a good yield of MXenes should be crucial for designing different MXene-based flexible batteries.

Improvement of the charge storage properties of MXenes is vital for high-performance flexible batteries. Combining MXenes with other electrode materials is a feasible and general scheme that can take advantage of high conductivity, good hydrophilicity, and large surface area. Many of these combinations have improved the battery performance in different aspects, including capacity, rate capability, cycling stability, energy, and power densities. However, most of these studies used MXenes or MXene-based composites as the negative electrode (anode) in batteries because they usually show an operation voltage of less than 1 V versus Li^+/Li. By exploiting diverse surface chemistries of MXenes, it is possible to use MXenes as positive electrodes (cathode). However, the transition of MXenes into metal oxides needs to be avoided.

MXenes have been widely used in different types of batteries, but the application of MXene-based flexible batteries in flexible electronics is actually in an initial stage because the performance of most flexible batteries is still far from satisfactory. For example, the cycling stability in a static state is much better than that after repeated deformations. The potential of MXenes can be explored further since the rich surface chemistry of MXenes enables additional functionalities. Such extensibility of MXenes will be helpful for MXene-based flexible batteries to realize some practical functions besides energy storage, for example, self-healing properties. However, the prototypes of related batteries are rarely seen, though some functional MXenes have already been synthesized and used in certain fields.

A complete system with MXene-based electronics and batteries has not yet been developed, which is primarily because the techniques differ from each other so much. Batteries are often fabricated by wet processes (e.g., coating of electrode slurries and adding liquid electrolytes). On the contrary, for electronics, a dry operation environment is preferred. To complete a system composed entirely of MXene, both battery and electronics preparation requirements need to be taken into account. A solid electrolyte, or at least a polymer electrolyte that does not leak liquid, would be a good choice for this flexible integrated system. Besides the fabrication of the integrated systems, the battery module needs to exactly match the power requirement of electronic modules to guarantee the practical operation. Owing to the diverse properties of MXenes, it is also possible to develop multifunctional MXene-based electrodes to realize a highly integrated system. We hope that this article will stimulate more systematic thinking about the use of MXenes in flexible electronics.

ACKNOWLEDGMENTS

Minshen Zhu acknowledges the support of the German Research Foundation DFG (ZH 989/2-1). Yang Huang is grateful for the support of the National Natural Science Foundation of China (grant no. 52002247) and the Natural Science Foundation of Guangdong Province (grant no. 2019A1515011344).

CONFLICTS OF INTEREST

The authors declare no conflicts of interest.

ORCID

Yang Huang https://orcid.org/0000-0001-5060-3414
Qiongqiong Lu http://orcid.org/0000-0001-6998-6275
Minshen Zhu http://orcid.org/0000-0001-5883-4962

REFERENCES

1. Geim AK, Novoselov KS. The rise of graphene. *Nat Mater*. 2007;6(3):183-191.
2. Rao CNR, Sood AK, Subrahmanyam KS, Govindaraj A. Graphene: the new two-dimensional nanomaterial. *Angew Chem Int Ed*. 2009;48(42):7752-7777.
3. Bhimanapati GR, Lin Z, Meunier V, et al. Recent advances in two-dimensional materials beyond graphene. *ACS Nano*. 2015;9(12):11509-11539.
4. Huang Y, Chen W, Li H, et al. Graphene stirrer with designed movements: targeting on environmental remediation and supercapacitor applications. *Green Energy Environ*. 2018;3(1):86-96.
5. Huang Y, Zhu M, Meng W, et al. Robust reduced graphene oxide paper fabricated with a household non-stick frying pan:

a large-area freestanding flexible substrate for supercapacitors. *RSC Adv*. 2015;5(43):33981-33989.

6. Yang S, Zhang P, Nia AS, Feng X. Emerging 2D materials produced *via* electrochemistry. *Adv Mater*. 2020;32(10):1907857.
7. Lei W, Mochalin VN, Liu D, Qin S, Gogotsi Y, Chen Y. Boron nitride colloidal solutions, ultralight aerogels and freestanding membranes through one-step exfoliation and functionalization. *Nat Commun*. 2015;6:8849.
8. Manzeli S, Ovchinnikov D, Pasquier D, Yazyev OV, Kis A. 2D transition metal dichalcogenides. *Nat Rev Mater*. 2017;2(8):17033.
9. Luo S, Zhao J, Zou J, et al. Self-standing polypyrrole/black phosphorus laminated film: promising electrode for flexible supercapacitor with enhanced capacitance and cycling stability. *ACS Appl Mater Interfaces*. 2018;10(4):3538-3548.
10. Kang J, Wood JD, Wells SA, et al. Solvent exfoliation of electronic-grade, two-dimensional black phosphorus. *ACS Nano*. 2015;9(4):3596-3604.
11. Dong R, Han P, Arora H, et al. High-mobility band-like charge transport in a semiconducting two-dimensional metal–organic framework. *Nat Mater*. 2018;17(11):1027-1032.
12. Liu K, Qi H, Dong R, et al. On-water surface synthesis of crystalline, few-layer two-dimensional polymers assisted by surfactant monolayers. *Nat Chem*. 2019;11(11):994-1000.
13. Choi W, Choudhary N, Han GH, Park J, Akinwande D, Lee YH. Recent development of two-dimensional transition metal dichalcogenides and their applications. *Mater Today*. 2017;20(3):116-130.
14. Naguib M, Kurtoglu M, Presser V, et al. Two-dimensional nanocrystals produced by exfoliation of Ti_3AlC_2. *Adv Mater*. 2011;23(37):4248-4253.
15. Xu B, Gogotsi Y. MXenes—the fastest growing materials family in the two-dimensional world. *Chin Chem Lett*. 2020;31(4):919-921.
16. Anasori B, Lukatskaya MR, Gogotsi Y. 2D metal carbides and nitrides (MXenes) for energy storage. *Nat Rev Mater*. 2017;2(2):16098.
17. Frey NC, Wang J, Vega Bellido GI, Anasori B, Gogotsi Y, Shenoy VB. Prediction of synthesis of 2D metal carbides and nitrides (MXenes) and their precursors with positive and unlabeled machine learning. *ACS Nano*. 2019;13(3):3031-3041.
18. Naguib M, Mochalin VN, Barsoum MW, Gogotsi Y. 25th anniversary article: MXenes: a new family of two-dimensional materials. *Adv Mater*. 2014;26(7):992-1005.
19. VahidMohammadi A, Rosen J, Gogotsi Y. The world of two-dimensional carbides and nitrides (MXenes). *Science*. 2021;372(6547):eabf1581.
20. Kamysbayev V, Filatov AS, Hu H, et al. Covalent surface modifications and superconductivity of two-dimensional metal carbide MXenes. *Science*. 2020;369(6506):979-983.
21. Khazaei M, Ranjbar A, Arai M, Sasaki T, Yunoki S. Electronic properties and applications of MXenes: a theoretical review. *J Mater Chem C*. 2017;5(10):2488-2503.
22. Mathis TS, Maleski K, Goad A, et al. Modified MAX phase synthesis for environmentally stable and highly conductive Ti_3C_2 MXene. *ACS Nano*. 2021;15(4):6420-6429.
23. Zhang C, Cui L, Abdolhosseinzadeh S, Heier J. Two-dimensional MXenes for lithium-sulfur batteries. *InfoMat*. 2020;2(4):613-638.
24. Okubo M, Sugahara A, Kajiyama S, Yamada A. MXene as a charge storage host. *Acc Chem Res*. 2018;51(3):591-599.
25. Ming F, Liang H, Huang G, Bayhan Z, Alshareef HN. MXenes for rechargeable batteries beyond the lithium-ion. *Adv Mater*. 2021;33(1):2004039.
26. Dong Y, Shi H, Wu Z-S. Recent advances and promise of MXene-based nanostructures for high-performance metal ion batteries. *Adv Funct Mater*. 2020;30(47):2000706.
27. Sun N, Zhu Q, Anasori B, et al. MXene-bonded flexible hard carbon film as anode for stable Na/K-ion storage. *Adv Funct Mater*. 2019;29(51):1906282.
28. Zhu M, Huang Y, Deng Q, et al. Highly flexible, freestanding supercapacitor electrode with enhanced performance obtained by hybridizing polypyrrole chains with MXene. *Adv Energy Mater*. 2016;6(21):1600969.
29. Liu Y, Dai Z, Zhang W, et al. Sulfonic-group-grafted $Ti_3C_2T_x$ MXene: a silver bullet to settle the instability of polyaniline toward high-performance Zn-ion batteries. *ACS Nano*. 2021;15(5):9065-9075.
30. Peng J, Chen X, Ong W-J, Zhao X, Li N. Surface and heterointerface engineering of 2D MXenes and their nanocomposites: insights into electro- and photocatalysis. *Chem*. 2019;5(1):18-50.
31. Shahzad F, Alhabeb M, Hatter CB, et al. Electromagnetic interference shielding with 2D transition metal carbides (MXenes). *Science*. 2016;353(6304):1137-1140.
32. Huang K, Li Z, Lin J, Han G, Huang P. Two-dimensional transition metal carbides and nitrides (MXenes) for biomedical applications. *Chem Soc Rev*. 2018;47(14):5109-5124.
33. Luo S, Xie L, Han F, et al. Nanoscale parallel circuitry based on interpenetrating conductive assembly for flexible and high-power zinc ion battery. *Adv Funct Mater*. 2019;29(28):1901336.
34. Zhang W, Peng J, Hua W, et al. Architecting amorphous vanadium oxide/MXene nanohybrid *via* tunable anodic oxidation for high-performance sodium-ion batteries. *Adv Energy Mater*. 2021;11(22):2100757.
35. Liu Y, Jiang Y, Hu Z, et al. *In-situ* electrochemically activated surface vanadium valence in V_2C MXene to achieve high capacity and superior rate performance for Zn-ion batteries. *Adv Funct Mater*. 2020;31(8):2008033.
36. Zhang N, Huang S, Yuan Z, Zhu J, Zhao Z, Niu Z. Direct self-assembly of MXene on Zn anodes for dendrite-free aqueous zinc-ion batteries. *Angew Chem Int Ed*. 2021;60(6):2861-2865.
37. Gu J, Zhu Q, Shi Y, et al. Single zinc atoms immobilized on MXene ($Ti_3C_2Cl_x$) layers toward dendrite-free lithium metal anodes. *ACS Nano*. 2020;14(1):891-898.
38. Wang Y, Zheng Y, Zhao J, Li Y. Assembling free-standing and aligned tungstate/MXene fiber for flexible lithium and sodium-ion batteries with efficient pseudocapacitive energy storage. *Energy Storage Mater*. 2020;33:82-87.
39. Li Y, Yang H, Zhang T, et al. Stretchable Zn-ion hybrid battery with reconfigurable V_2CT_x and $Ti_3C_2T_x$ MXene electrodes as a magnetically actuated soft robot. *Adv Energy Mater*. 2021;11(45):2101862.
40. Yang Q, Xu Z, Fang B, et al. MXene/graphene hybrid fibers for high performance flexible supercapacitors. *J Mater Chem A*. 2017;5(42):22113-22119.

41. Fu Z, Wang N, Legut D, et al. Rational design of flexible two-dimensional MXenes with multiple functionalities. *Chem Rev*. 2019;119(23):11980-12031.
42. Gao L, Li C, Huang W, et al. MXene/polymer membranes: synthesis, properties, and emerging applications. *Chem Mater*. 2020;32(5):1703-1747.
43. Zhang K, Sun J, Song J, et al. Self-healing Ti_3C_2 MXene/PDMS supramolecular elastomers based on small biomolecules modification for wearable sensors. *ACS Appl Mater Interfaces*. 2020;12(40):45306-45314.
44. Qin L, Jiang J, Tao Q, et al. A flexible semitransparent photovoltaic supercapacitor based on water-processed MXene electrodes. *J Mater Chem A*. 2020;8(11):5467-5475.
45. Jiang Q, Wu C, Wang Z, et al. MXene electrochemical microsupercapacitor integrated with triboelectric nanogenerator as a wearable self-charging power unit. *Nano Energy*. 2018;45:266-272.
46. Liu Y, Xiao H, Goddard WA. Schottky-barrier-free contacts with two-dimensional semiconductors by surface-engineered MXenes. *J Am Chem Soc*. 2016;138(49):15853-15856.
47. Urbankowski P, Anasori B, Makaryan T, et al. Synthesis of two-dimensional titanium nitride Ti_4N_3 (MXene). *Nanoscale*. 2016;8(22):11385-11391.
48. Halim J, Kota S, Lukatskaya MR, et al. Synthesis and characterization of 2D molybdenum carbide (MXene). *Adv Funct Mater*. 2016;26(18):3118-3127.
49. Anasori B, Shi C, Moon EJ, et al. Control of electronic properties of 2D carbides (MXenes) by manipulating their transition metal layers. *Nanoscale Horiz*. 2016;1(3):227-234.
50. Wei Y, Zhang P, Soomro RA, Zhu Q, Xu B. Advances in the synthesis of 2D MXenes. *Adv Mater*. 2021;33(39):2103148.
51. Wang H-W, Naguib M, Page K, Wesolowski DJ, Gogotsi Y. Resolving the structure of $Ti_3C_2T_x$ MXenes through multi-level structural modeling of the atomic pair distribution function. *Chem Mater*. 2016;28(1):349-359.
52. Hantanasirisakul K, Gogotsi Y. Electronic and optical properties of 2D transition metal carbides and nitrides (MXenes). *Adv Mater*. 2018;30(52):1804779.
53. Han F, Luo S, Xie L, et al. Boosting the yield of MXene 2D sheets *via* a facile hydrothermal-assisted intercalation. *ACS Appl Mater Interfaces*. 2019;11(8):8443-8452.
54. Huang X, Wu P. A Facile, High-yield, and freeze-and-thaw-assisted approach to fabricate MXene with plentiful wrinkles and its application in on-chip micro-supercapacitors. *Adv Funct Mater*. 2020;30(12):1910048.
55. Shuck CE, Sarycheva A, Anayee M, et al. Scalable synthesis of $Ti_3C_2T_x$ MXene. *Adv Eng Mater*. 2020;22(3):1901241.
56. Mashtalir O, Naguib M, Dyatkin B, Gogotsi Y, Barsoum MW. Kinetics of aluminum extraction from Ti_3AlC_2 in hydrofluoric acid. *Mater Chem Phys*. 2013;139(1):147-152.
57. Sang X, Xie Y, Lin M-W, et al. Atomic defects in monolayer titanium carbide ($Ti_3C_2T_x$) MXene. *ACS Nano*. 2016;10(10):9193-9200.
58. Alhabeb M, Maleski K, Anasori B, et al. Guidelines for synthesis and processing of two-dimensional titanium carbide ($Ti_3C_2T_x$ MXene). *Chem Mater*. 2017;29(18):7633-7644.
59. Naguib M, Barsoum MW, Gogotsi Y. Ten years of progress in the synthesis and development of MXenes. *Adv Mater*. 2021;33(39):2103393.
60. Hope MA, Forse AC, Griffith KJ, et al. NMR reveals the surface functionalisation of Ti_3C_2 MXene. *Phys Chem Chem Phys*. 2016;18(7):5099-5102.
61. Ghidiu M, Lukatskaya MR, Zhao M-Q, Gogotsi Y, Barsoum MW. Conductive two-dimensional titanium carbide 'clay' with high volumetric capacitance. *Nature*. 2014;516(7529):78-81.
62. Sun W, Shah SA, Chen Y, et al. Electrochemical etching of Ti_2AlC to Ti_2CT_x (MXene) in low-concentration hydrochloric acid solution. *J Mater Chem A*. 2017;5(41):21663-21668.
63. Yang S, Zhang P, Wang F, et al. Fluoride-free synthesis of two-dimensional titanium carbide (MXene) using a binary aqueous system. *Angew Chem Int Ed*. 2018;57(47):15491-15495.
64. Li T, Yao L, Liu Q, et al. Fluorine-free synthesis of high-purity $Ti_3C_2T_x$ (T=OH, O) *via* alkali treatment. *Angew Chem Int Ed*. 2018;57(21):6115-6119.
65. Halim J, Lukatskaya MR, Cook KM, et al. Transparent conductive two-dimensional titanium carbide epitaxial thin films. *Chem Mater*. 2014;26(7):2374-2381.
66. Natu V, Pai R, Sokol M, Carey M, Kalra V, Barsoum MW. 2D $Ti_3C_2T_z$ MXene synthesized by water-free etching of Ti_3AlC_2 in polar organic solvents. *Chem*. 2020;6(3):616-630.
67. Tang Q, Zhou Z, Shen P. Are MXenes promising anode materials for Li ion batteries? Computational studies on electronic properties and Li storage capability of Ti_3C_2 and $Ti_3C_2X_2$ (X = F, OH) monolayer. *J Am Chem Soc*. 2012;134(40):16909-16916.
68. Li Y, Shao H, Lin Z, et al. A general Lewis acidic etching route for preparing MXenes with enhanced electrochemical performance in non-aqueous electrolyte. *Nat Mater*. 2020;19(8):894-899.
69. Ahmed B, Anjum DH, Hedhili MN, Gogotsi Y, Alshareef HN. H_2O_2 assisted room temperature oxidation of Ti_2C MXene for Li-ion battery anodes. *Nanoscale*. 2016;8(14):7580-7587.
70. Tao Q, Dahlqvist M, Lu J, et al. Two-dimensional $Mo_{1.33}C$ MXene with divacancy ordering prepared from parent 3D laminate with in-plane chemical ordering. *Nat Commun*. 2017;8:14949.
71. Meshkian R, Dahlqvist M, Lu J, et al. W-based atomic laminates and their 2D derivative $W_{1.33}C$ MXene with vacancy ordering. *Adv Mater*. 2018;30(21):1706409.
72. Naguib M, Halim J, Lu J, et al. New Two-dimensional niobium and vanadium carbides as promising materials for Li-ion batteries. *J Am Chem Soc*. 2013;135(43):15966-15969.
73. VahidMohammadi A, Hadjikhani A, Shahbazmohamadi S, Beidaghi M. Two-dimensional vanadium carbide (MXene) as a high-capacity cathode material for rechargeable aluminum batteries. *ACS Nano*. 2017;11(11):11135-11144.
74. Soundiraraju B, George BK. Two-dimensional titanium nitride (Ti_2N) MXene: synthesis, characterization, and potential application as surface-enhanced Raman scattering substrate. *ACS Nano*. 2017;11(9):8892-8900.
75. Naguib M, Mashtalir O, Carle J, et al. Two-dimensional transition metal carbides. *ACS Nano*. 2012;6(2):1322-1331.
76. Zhao S, Meng X, Zhu K, et al. Li-ion uptake and increase in interlayer spacing of Nb_4C_3 MXene. *Energy Storage Mater*. 2017;8:42-48.
77. Tran MH, Schäfer T, Shahraei A, et al. Adding a new member to the MXene family: synthesis, structure, and electrocatalytic activity for the hydrogen evolution reaction of $V_4C_3T_x$. *ACS Appl Energy Mater*. 2018;1(8):3908-3914.

78. Anasori B, Xie Y, Beidaghi M, et al. Two-dimensional, ordered, double transition metals carbides (MXenes). *ACS Nano*. 2015;9(10):9507-9516.
79. Zhou J, Zha X, Chen FY, et al. A two-dimensional zirconium carbide by selective etching of Al_3C_3 from nanolaminated $Zr_3Al_3C_5$. *Angew Chem Int Ed*. 2016;55(16):5008-5013.
80. Zhou J, Zha X, Zhou X, et al. Synthesis and electrochemical properties of two-dimensional hafnium carbide. *ACS Nano*. 2017;11(4):3841-3850.
81. Halim J, Palisaitis J, Lu J, et al. Synthesis of two-dimensional $Nb_{1.33}C$ (MXene) with randomly distributed vacancies by etching of the quaternary solid solution $(Nb_{2/3}Sc_{1/3})_2AlC$ MAX Phase. *ACS Appl Nano Mater*. 2018;1(6):2455-2460.
82. Lipatov A, Alhabeb M, Lukatskaya MR, Boson A, Gogotsi Y, Sinitskii A. Effect of synthesis on quality, electronic properties and environmental stability of individual monolayer Ti_3C_2 MXene Flakes. *Adv Electron Mater*. 2016;2(12):1600255.
83. Peng C, Wei P, Chen X, et al. A hydrothermal etching route to synthesis of 2D MXene (Ti_3C_2, Nb_2C): enhanced exfoliation and improved adsorption performance. *Ceram Int*. 2018;44(15):18886-18893.
84. Liu F, Zhou J, Wang S, et al. Preparation of high-purity V_2C MXene and electrochemical properties as Li-ion batteries. *J Electrochem Soc*. 2017;164(4):A709-A713.
85. Wu M, Wang B, Hu Q, Wang L, Zhou A. The synthesis process and thermal stability of V_2C MXene. *Materials*. 2018;11(11):2112.
86. Liu F, Zhou A, Chen J, et al. Preparation of Ti_3C_2 and Ti_2C MXenes by fluoride salts etching and methane adsorptive properties. *Appl Surf Sci*. 2017;416:781-789.
87. Wang L, Zhang H, Wang B, et al. Synthesis and electrochemical performance of $Ti_3C_2T_x$ with hydrothermal process. *Electron Mater Lett*. 2016;12(5):702-710.
88. Li M, Lu J, Luo K, et al. Element replacement approach by reaction with Lewis acidic molten salts to synthesize nanolaminated MAX Phases and MXenes. *J Am Chem Soc*. 2019;141(11):4730-4737.
89. Mashtalir O, Naguib M, Mochalin VN, et al. Intercalation and delamination of layered carbides and carbonitrides. *Nat Commun*. 2013;4:1716.
90. Naguib M, Unocic RR, Armstrong BL, Nanda J. Large-scale delamination of multi-layers transition metal carbides and carbonitrides "MXenes". *Dalton Trans*. 2015;44(20):9353-9358.
91. Wu W, Xu J, Tang X, et al. Two-dimensional nanosheets by rapid and efficient microwave exfoliation of layered materials. *Chem Mater*. 2018;30(17):5932-5940.
92. Shi YE, Han F, Xie L, et al. A MXene of type $Ti_3C_2T_x$ functionalized with copper nanoclusters for the fluorometric determination of glutathione. *Mikrochim Acta*. 2019;187(1):38.
93. Zhang CJ, Pinilla S, McEvoy N, et al. Oxidation stability of colloidal two-dimensional titanium carbides (MXenes). *Chem Mater*. 2017;29(11):4848-4856.
94. Malaki M, Maleki A, Varma RS. MXenes and ultrasonication. *J Mater Chem A*. 2019;7(18):10843-10857.
95. Zhang Q, Lai H, Fan R, Ji P, Fu X, Li H. High concentration of $Ti_3C_2T_x$ MXene in organic solvent. *ACS Nano*. 2021;15(3):5249-5262.
96. Seyedin S, Zhang J, Usman KAS, et al. Facile solution processing of stable MXene dispersions towards conductive composite fibers. *Global Challenges*. 2019;3(10):1900037.
97. Zhao M-Q, Xie X, Ren CE, et al. Hollow MXene spheres and 3D macroporous MXene frameworks for Na-ion storage. *Adv Mater*. 2017;29(37):1702410.
98. Shin H, Eom W, Lee KH, Jeong W, Kang DJ, Han TH. Highly electroconductive and mechanically strong $Ti_3C_2T_x$ MXene fibers using a deformable MXene fel. *ACS Nano*. 2021;15(2):3320-3329.
99. Zhang J, Seyedin S, Qin S, et al. Highly Conductive $Ti_3C_2T_x$ MXene hybrid fibers for flexible and elastic fiber-shaped supercapacitors. *Small*. 2019;15(8):1804732.
100. Bi L, Yang Z, Chen L, Wu Z, Ye C. Compressible AgNWs/$Ti_3C_2T_x$ MXene aerogel-based highly sensitive piezoresistive pressure sensor as versatile electronic skins. *J Mater Chem A*. 2020;8(38):20030-20036.
101. Chang K, Li L, Zhang C, et al. Compressible and robust PANI sponge anchored with erected MXene flakes for human motion detection. *Compos. Part A Appl Sci Manuf* 2021;151:106671.
102. Cao Z, Zhu Q, Wang S, et al. Perpendicular MXene arrays with periodic interspaces toward dendrite-free lithium metal anodes with high-rate capabilities. *Adv Funct Mater*. 2020;30(5):1908075.
103. Xia Y, Mathis TS, Zhao M-Q, et al. Thickness-independent capacitance of vertically aligned liquid-crystalline MXenes. *Nature*. 2018;557(7705):409-412.
104. Yan J, Ren CE, Maleski K, et al. Flexible MXene/graphene films for ultrafast supercapacitors with outstanding volumetric capacitance. *Adv Funct Mater*. 2017;27(30):1701264.
105. Wang H, Li J, Kuai X, et al. Enhanced rate capability of ion-accessible $Ti_3C_2T_x$-NbN hybrid electrodes. *Adv Energy Mater*. 2020;10(35):2001411.
106. Tang J, Mathis TS, Kurra N, et al. Tuning the electrochemical performance of titanium carbide MXene by controllable *in situ* anodic oxidation. *Angew Chem Int Ed*. 2019;58(49):17849-17855.
107. Tang J, Mathis T, Zhong X, et al. Optimizing ion pathway in titanium carbide MXene for practical high-rate supercapacitor. *Adv Energy Mater*. 2021;11(4):2003025.
108. Li G, Wyatt BC, Song F, et al. 2D titanium carbide (MXene) based films: expanding the frontier of functional film materials. *Adv Funct Mater*. 2021;31(46):2105043.
109. Pang J, Mendes RG, Bachmatiuk A, et al. Applications of 2D MXenes in energy conversion and storage systems. *Chem Soc Rev*. 2019;48(1):72-133.
110. Aslam MK, Niu Y, Xu M. MXenes for non-lithium-ion (Na, K, Ca, Mg, and Al) batteries and supercapacitors. *Adv Energy Mater*. 2021;11(2):2000681.
111. Li K, Liang M, Wang H, et al. 3D MXene architectures for efficient energy storage and conversion. *Adv Funct Mater*. 2020;30(47):2000842.
112. Hui X, Ge X, Zhao R, Li Z, Yin L. Interface chemistry on MXene-based materials for enhanced energy storage and conversion performance. *Adv Funct Mater*. 2020;30(50):2005190.
113. Li X, Ma X, Hou Y, et al. Intrinsic voltage plateau of a Nb_2CT_x MXene cathode in an aqueous electrolyte induced by high-voltage scanning. *Joule*. 2021;5(11):2993-3005.
114. Li X, Li M, Huang Z, et al. Activating the I^0/I^+ redox couple in an aqueous I_2–Zn battery to achieve a high voltage plateau. *Energy Environ Sci*. 2021;14(1):407-413.
115. Zhao Q, Zhu Q, Liu Y, Xu B. Status and prospects of MXene-based lithium–sulfur batteries. *Adv Funct Mater*. 2021;31(21):2100457.

116. Zhang D, Wang S, Hu R, et al. Catalytic conversion of polysulfides on single atom zinc implanted MXene toward high-rate lithium–sulfur batteries. *Adv Funct Mater*. 2020; 30(30):2002471.
117. Sun C, Shi X, Zhang Y, Liang J, Qu J, Lai C. $Ti_3C_2T_x$ MXene interface layer driving ultra-stable lithium-iodine batteries with both high iodine content and mass loading. *ACS Nano*. 2020;14(1):1176-1184.
118. Li X, Li N, Huang Z, et al. Enhanced redox kinetics and duration of aqueous I^2/I^- conversion chemistry by MXene confinement. *Adv Mater*. 2021;33(8):2006897.
119. Tang H, Qu Z, Yan Y, et al. Unleashing energy storage ability of aqueous battery electrolytes. *Mater Futures*. In press; doi:10.1088/2752–5724/ac52e8
120. Hadler-Jacobsen J, Fagerli FH, Kaland H, Schnell SK. Stacking sequence, interlayer bonding, termination group stability and Li/Na/Mg diffusion in MXenes. *ACS Mater Lett*. 2021;3(9):1369-1376.
121. Pei Y, Zhang X, Hui Z, et al. $Ti_3C_2T_x$ MXene for sensing applications: recent progress, design principles, and future perspectives. *ACS Nano*. 2021;15(3):3996-4017.
122. Pu J-H, Zhao X, Zha X-J, et al. Multilayer structured AgNW/WPU-MXene fiber strain sensors with ultrahigh sensitivity and a wide operating range for wearable monitoring and healthcare. *J Mater Chem A*. 2019;7(26):15913-15923.
123. Cheng Y, Ma Y, Li L, et al. Bioinspired microspines for a high-performance spray $Ti_3C_2T_x$ MXene-based piezoresistive sensor. *ACS Nano*. 2020;14(2):2145-2155.
124. Yu X-F, Li Y-C, Cheng J-B, et al. Monolayer Ti_2CO_2: a promising candidate for NH_3 sensor or capturer with high sensitivity and selectivity. *ACS Appl Mater Interfaces*. 2015; 7(24):13707-13713.
125. Lee E, VahidMohammadi A, Prorok BC, Yoon YS, Beidaghi M, Kim D-J. Room temperature gas sensing of two-dimensional titanium carbide (MXene). *ACS Appl Mater Interfaces*. 2017;9(42):37184-37190.
126. Römer FM, Wiedwald U, Strusch T, et al. Controlling the conductivity of Ti_3C_2 MXenes by inductively coupled oxygen and hydrogen plasma treatment and humidity. *RSC Adv*. 2017;7(22):13097-13103.
127. Wang Z, Yu K, Feng Y, Qi R, Ren J, Zhu Z. Stabilizing $Ti_3C_2T_x$-MXenes with $TiOF_2$ nanospheres intercalation to improve hydrogen evolution reaction and humidity-sensing performance. *Appl Surf Sci*. 2019;496:143729.
128. Zhang Y, Jiang X, Zhang J, Zhang H, Li Y. Simultaneous voltammetric determination of acetaminophen and isoniazid using MXene modified screen-printed electrode. *Biosens Bioelectron*. 2019;130:315-321.
129. Wang H, Li H, Huang Y, Xiong M, Wang F, Li C. A label-free electrochemical biosensor for highly sensitive detection of gliotoxin based on DNA nanostructure/MXene nanocomplexes. *Biosens Bioelectron*. 2019;142:111531.
130. Xu B, Zhu M, Zhang W, et al. Ultrathin MXene-micropattern-based field-effect transistor for probing neural activity. *Adv Mater*. 2016;28(17):3333-3339.
131. Lyu B, Kim M, Jing H, et al. Large-area MXene electrode array for flexible electronics. *ACS Nano*. 2019;13(10): 11392-11400.
132. Xu X, Guo T, Hota MK, et al. High-yield $Ti_3C_2T_x$ MXene–MoS_2 integrated circuits. *Adv Mater*. 2021: 2107370.
133. Wang Z, Kim H, Alshareef HN. Oxide thin-film electronics using all-MXene electrical contacts. *Adv Mater*. 2018;30(15): 1706656.
134. Lai S, Jang SK, Cho JH, Lee S. Organic field-effect transistors integrated with Ti_2CT_x electrodes. *Nanoscale*. 2018;10(11): 5191-5197.
135. Xu J, Shim J, Park J-H, Lee S. MXene electrode for the integration of WSe_2 and MoS_2 field effect transistors. *Adv Funct Mater*. 2016;26(29):5328-5334.
136. Kim H, Nugraha MI, Guan X, et al. All-solution-processed quantum dot electrical double-layer transistors enhanced by surface charges of $Ti_3C_2T_x$ MXene contacts. *ACS Nano*. 2021; 15(3):5221-5229.
137. Sarycheva A, Polemi A, Liu Y, Dandekar K, Anasori B, Gogotsi Y. 2D titanium carbide (MXene) for wireless communication. *Sci Adv*. 2018;4(9):eaau0920.
138. Han M, Liu Y, Rakhmanov R, et al. Solution-processed $Ti_3C_2T_x$ MXene antennas for radio-frequency communication. *Adv Mater*. 2021;33(1):2003225.
139. Li X, Li Q, Hou Y, et al. Toward a practical Zn powder anode: $Ti_3C_2T_x$ MXene as a lattice-match electrons/ions redistributor. *ACS Nano*. 2021;15(9):14631-14642.

AUTHOR BIOGRAPHIES

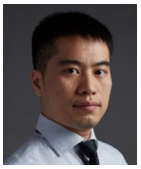

Yang Huang was awarded his Ph.D. degree in Philosophy from the City University of Hong Kong in 2016. He is currently an assistant professor in the College of Materials Science and Engineering, Shenzhen University. His research mainly focuses on low-dimensional materials (e.g., transition–metal carbides and nitrides, known as MXenes) and their applications in advanced micro-/nano electronic devices (e.g., battery and supercapacitor).

Qiongqiong Lu is currently a postdoctor at the Leibniz Institute for Solid State and Materials Research (IFW) Dresden, Germany. He received his Ph.D. degree at Dresden University of Technology (TU Dresden) in 2022 and MSc degree from Nankai University in 2017. His research focuses on functional materials for batteries.

Dianlun Wu was awarded his Bachelor's Degree from Guangdong University of Petrochemical Technology in 2018. He is currently a Master student in the College of Materials Science and Engineering, Shenzhen University. His research focuses on, and their applications in silver-zinc batteries.

Yue Jiang received his Master degree from Guangdong University of Technology in 2020. He was a research assistant in the College of Materials Science and Engineering, Shenzhen University. His research mainly focuses on aqueous batteries and low-dimensional devices.

Zhenjie Liu is a postdoctoral fellow in Shenzhen University and a visiting fellow in the University of Wollongong (UOW). He received his Ph.D. degree from School of Applied Chemistry and Engineering (Changchun Institute of Applied Chemistry Chinese Academy of Sciences) at University of Science and Technology of China in 2019. His current research focuses on the metal anodes for energy storage including alkali metal-ion and -oxygen batteries.

Bin Chen received his Ph.D. degree of Philosophy from Unverisyt of Groningen in 2017. He is currently an associate researcher in the College of Materials Science and Engineering, Shenzhen University. His research mainly focuses on low-dimensional devices and their applications in volatile/nonvolatile memories.

Minshen Zhu received his Ph.D. degree from the City University of Hong Kong, in 2017. He subsequently joined the Institute for Integrative Nanosciences at Leibniz IFW Dresden and led the research of energy storage at the microscale. In 2022, he moved to the Research Center for Materials, Architectures, and Integration of Nanomembranes (MAIN) at Chemnitz University of Technology. Supported by the European Research Council (Starting Grant), his research activities aim to develop on-chip manufacturable dust-sized batteries for monolithic integration in intelligent microsystems.

Oliver G. Schmidt received the Dr.rer.-nat. degree from TU Berlin in 1999. From 2007 to 2021, he was the Director of the Institute for Integrative Nanosciences at Leibniz IFW Dresden. He holds a Full Professorship for Materials Systems for Nanoelectronics and is the Scientific Director of the Research Center for Materials, Architectures and Integration of Nanomembranes (MAIN) at Chemnitz University of Technology. He is an Adjunct Professor for Nanophysics at TU Dresden and holds an Honorary Professorship at Fudan University. His interdisciplinary activities bridge across several research fields, ranging from energy storage and flexible electronics to microrobotics and nanophotonics.

How to cite this article: Huang Y, Lu Q, Wu D, et al. Flexible MXene films for batteries and beyond. *Carbon Energy*. 2022;1-23. doi:10.1002/cey2.200